

Equilibrium partitioning and subsequent re-distribution of halogens among apatite–biotite–amphibole assemblages from mantle-derived plutonic rocks: Complexities revealed

Holger Teiber ^a, Manuel Scharrer ^a, Michael A.W. Marks ^{a,*}, Andrei A. Arzamastsev ^{b,c}, Thomas Wenzel ^a, Gregor Markl ^a

^a Eberhard-Karls Universität Tübingen, Mathematisch-Naturwissenschaftliche Fakultät, FB Geowissenschaften, Wilhelmstraße 56, D-72074 Tübingen, Germany

^b Institute of Precambrian Geology and Geochronology RAS, Makarova Emb. 2, St. Petersburg 199034, Russia

^c St. Petersburg State University, Universitetskaya Emb., 7/9, St. Petersburg 199034, Russia



ARTICLE INFO

Article history:

Received 21 October 2014

Accepted 11 February 2015

Available online 21 February 2015

Keywords:

Halogen distribution

Apatite

Biotite

Amphibole

Equilibrium partitioning

Re-distribution

ABSTRACT

The concentration of halogens in apatite, biotite and amphibole is investigated for a large variety of mantle-derived plutonic rocks (gabbros, diorites, monzonites, olivine- and pyroxene-bearing monzonitic to granitic rocks, syenites, carbonatites and a phoscorite). In all rocks studied, apatite occurs as an early magmatic phase, whereas biotite and amphibole may occur either as a late magmatic phase or as late-stage, potentially hydrothermal product replacing precursor olivine, pyroxene and Fe-Ti oxides (ilmenite and magnetite).

Based on electron microprobe analyses for F and Cl and detailed textural observations, we test existing models of halogen partitioning between apatite and biotite. Bromine concentration data for apatite, biotite and amphibole are used to further refine our understanding of the geochemical similarities and differences between Cl and Br during magmatic and hydrothermal processes.

Our data suggests that F and Cl contents in apatite, biotite and amphibole can indeed be useful monitors of the halogen systematics in magmas, but they may also be subject to post-magmatic changes to variable extents. The relatively small radius and compatible F cation seems to be less prone to post-magmatic alteration and is likely to best reflect the original magmatic halogen abundances – especially in apatite. However, the larger and probably more incompatible Cl anion, is more easily re-mobilized as reflected by strong redistribution of Cl in biotite and amphibole which have been clearly overprinted by hydrothermal fluids. In certain cases, the ability of halogens to re-distribute themselves after magmatic equilibrium partitioning (as emphasized by our data) suggests that observed partitioning (especially between apatite and biotite) may also be used as a very sensitive indicator for post-magmatic hydrothermal processes.

© 2015 Elsevier B.V. All rights reserved.

1. Introduction

Halogens (F, Cl and Br) influence the physical properties of natural melts (e.g., density, viscosity and crystallization temperature) and are important for many magmatic and hydrothermal processes such as the transport of metals in melts and hydrothermal fluids. Their potential environmental impacts are related to volcanic eruptions due to the release of these elements into the atmosphere (see the recent reviews of Aiuppa et al., 2009; Pyle and Mather, 2009).

In most plutonic rocks apatite, micas and amphibole are the major halogen-bearing phases (e.g., Speer, 1984; Markl and Piazolo, 1998; Piccoli and Candela, 2002; Zhang et al., 2012; Teiber et al., 2014), although titanite, fluorite, topaz, epidote, sodalite or scapolite may be important in some cases (Breiter and Siebel, 1995; Teertstra and Sherriff, 1997; Förster

et al., 1999; Frost et al., 2000; Frindt et al., 2004; Gieré and Sorensen, 2004; Krumrei et al., 2007; Gioncada et al., 2014). Because of the similar ionic radii of F⁻ (1.33 Å; Shannon, 1976) and OH⁻ (1.32–1.37 Å), F⁻ is much easily incorporated into OH-bearing minerals than the larger Cl⁻ (1.81 Å) and Br⁻ (1.95 Å). Consequently, in mineral-melt systems, F is less incompatibly during magmatic differentiation than the heavier halogens Cl and Br (e.g., Pyle and Mather, 2009). Furthermore, in melt-fluid systems, Cl and Br preferentially partition into the fluid phase, whereas F is largely retained in the melt, resulting in the fractionation of F from Cl and Br during fluid-present magmatic processes (e.g., Fuge, 1977; Webster and Holloway, 1990; Carroll and Webster, 1994; Villemant and Boudon, 1999; Bureau et al., 2000; Webster et al., 2009; Wang et al., 2014a).

Several studies have addressed the partitioning of F and Cl in melt-mineral-fluid systems and models have been developed to reconstruct F and Cl concentrations in melts and fluids using the halogen contents in apatite, biotite and amphibole to monitor the process (e.g., Stormer and

* Corresponding author.

E-mail address: michael.marks@uni-tuebingen.de (M.A.W. Marks).

Carmichael, 1971; Westrich, 1981; Munoz, 1984; Volfing et al., 1985; Zhu and Sverjensky, 1991, 1992; Brenan, 1993; Icenhower and London, 1997; Villemant and Boudon, 1999; Piccoli and Candela, 2002; Mathez and Webster, 2005; Boyce and Hervig, 2008; Chevchelov et al., 2008; Webster et al., 2009; Patiño Douce et al., 2011; Zhang et al., 2012; Teiber et al., 2014). These studies show that F and Cl contents in apatite, biotite and amphibole are governed by several factors such as, melt composition, crystallization temperature, the presence of a fluid phase and the major element composition of biotite and amphibole. These factors are commonly interconnected, since relatively primitive rocks (e.g., gabbros) normally have relatively high Mg contents and crystallize at higher temperatures compared to more evolved rocks such as many granites. As a result the respective Mg-numbers of hydroxyl-bearing silicates may influence their ability to incorporate halogens in these two different magma types. Also, the degree of differentiation of a melt governs the relative abundance of F and Cl to a certain extent, Cl becoming relatively depleted compared to F during late-magmatic or hydrothermal stages due to its strong affinity for an evolving fluid phase (e.g., Zhang et al., 2012). Finally, it has been suggested that halogens may be re-distributed between apatite and hydroxyl-bearing silicates as a consequence of late-stage or post-magmatic hydrothermal fluid circulation (e.g., Brenan, 1994; Willmore et al., 2000; Teiber et al., 2014). Despite these potential complexities, studies generally show that F/OH and Cl/OH ratios are normally higher in apatite than in biotite and amphibole from the same rock. Also, amphibole tends to display higher F/OH than associated biotite, but for Cl/OH ratios to not show such a clear relationship (e.g., Stormer and Carmichael, 1971; Ekström, 1972; Westrich, 1981; Volfing et al., 1985; Léger et al., 1996; Zhang et al., 2012; Teiber et al., 2014). Br is present at much lower concentrations than F & Cl, and there is little data for the distribution of this element, mainly due to analytical limitations (Ionov et al., 1997; O'Reilly and Griffin, 2000; Marks et al., 2012; Teiber et al., 2014; Wang et al., 2014b).

In the present study we have carefully measured the distribution of halogens (F, Cl and Br) between apatite, biotite and amphibole for a range of plutonic rocks including gabbros, diorites, monzonites, olivine- and pyroxene-bearing monzonitic to granitic rocks, syenites, carbonatites and a phoscorite. All rocks contain magmatic apatite that is clearly formed at an early stage in the crystallization sequence. Biotite and amphibole occur as subhedral to euhedral, probably magmatic phases and/or as texturally late overgrowths and reaction rims around orthomagmatic olivine and Fe-Ti oxides and/or as a replacement of pyroxene. This diversity allows us to investigate (i) the general applicability of existing halogen partitioning models between apatite and biotite and (ii) the potential susceptibility to alteration of magmatic halogen distribution patterns between apatite and hydroxyl-bearing silicates under late-magmatic to hydrothermal conditions during the final cooling of plutonic rocks. The combination of detailed textural observations with halogen distribution systematics allows us to distinguish the various episodes of halogen mobilization and the “footprint” of such events in the various minerals. Interpretation of these events is a prerequisite for modeling halogen distribution for an evolving magmatic-hydrothermal system.

2. Material and methods

The rock samples studied here are from five different localities. Selection was based on the abundance of apatite and most of them were previously investigated in previous petrological and geochemical studies (Table 1). Here we provide brief descriptions of geological settings and textures with a main focus on apatite, biotite and amphibole. A more detailed classification of apatite, biotite and amphibole group minerals is provided in Table 2.

2.1. Mont Saint-Hilaire

The Mont Saint-Hilaire complex (Canada) is one of many Cretaceous intrusive complexes of the alkaline Monteregian Hills Province and

consists of gabbros, diorites and foid syenites, that crystallized from partial melts of an OIB-type mantle source (e.g., Eby, 1985; Currie et al., 1986; Foland et al., 1988; Darbyshire et al., 2007; Schilling et al., 2011b).

We investigate two gabbroic (MSH17 and 18) and three dioritic (MSH12, 75 and 119) samples, which contain variable amounts of plagioclase, alkali feldspar, nepheline, olivine, clinopyroxene, Fe-Ti oxides, apatite, amphibole and biotite. Typical accessories are baddeleyite/zircon and pyrrhotite (Table 1). Apatite occurs in all samples as sub- to euhedral inclusions (20–300 µm) in orthomagmatic olivine, clinopyroxene and Fe-Ti oxides. Where present, biotite and amphibole appear as mm sized, subhedral grains (presumably magmatic) and as texturally late, fine-grained reaction rims around Fe-Ti oxides in contact with feldspar and in places intergrown with each other. Amphibole further occurs as replacement of pyroxene (Fig. 1a–c).

2.2. Ilímaussaq

The Ilímaussaq complex (South Greenland) is part of the Mid-Proterozoic alkaline Gardar Province. Its major rock units comprise augite syenites, peralkaline granites and nepheline syenites. Melting of lithospheric mantle followed by prolonged fractionation processes is assumed to be responsible for the origin of these rocks (e.g., Larsen and Sørensen, 1987; Marks and Markl, 2001, in press; Marks et al., 2004a, 2004b; Upton, 2013).

Five samples of augite syenite were chosen for this study, representing a traverse from the fine-grained margin (GM1858) towards the central part of the complex (GM1333, 1332, 1330 and 1857; see details in Marks and Markl, 2001; Zirner et al., submitted). They consist of apatite, alkali feldspar ± nepheline, olivine, clinopyroxene, Fe-Ti oxides, amphibole and biotite along with accessory baddeleyite/zircon, and pyrite ± pyrrhotite. All samples contain euhedral apatite (50–700 µm) enclosed in alkali feldspar, olivine, clinopyroxene, Fe-Ti oxides, amphibole and biotite (Fig. 1d–f). Brown amphibole occurs as poikilitic grains up to 3 mm in size, usually associated with alkali feldspar, apatite and Fe-Ti oxides (Fig. 1f). Red amphibole is present as a replacement of clinopyroxene and as fine-grained reaction rims around Fe-Ti oxides (in the latter case often associated with fine-grained biotite). A green amphibole forms and overgrows on olivine, and in places is intergrown with tiny biotite flakes (Fig. 1g–i).

2.3. Ardnamurchan

The Ardnamurchan complex (Scotland) is part of the Paleogene North Atlantic magmatic province and mainly consists of gabbroic and monzonitic rocks. The rocks formed by combined fractional crystallization of a tholeiitic magma and assimilation of country rocks (Walsh, 1975; Walsh and Henderson, 1977; Geldmacher et al., 1998; Emeleus and Bell, 2005; O'Driscoll, 2007).

For this study a monzonite (ARD16) and a quartz-monzonite (ARD17) were investigated in detail. Both rock samples consist of plagioclase, alkali-feldspar, quartz, Fe-Ti oxides and apatite. ARD16 contains additional clinopyroxene, amphibole and rare biotite. In contrast, ARD17 is rich in biotite but lacks amphibole. Apatite in both samples (10–300 µm) occurs as euhedral to subhedral inclusions in feldspars, Fe-Ti oxides and in biotite and amphibole, if present. Euhedral to subhedral biotite (up to several mm) in ARD17 (0.2–3 mm) and subhedral amphibole (0.2–1.5 mm) and rare subhedral biotite (0.2 mm) in ARD16 appear to be of magmatic origin (Fig. 1j and k). Additionally, ARD16 contains abundant fine-grained reaction rims of biotite surrounding Fe-Ti oxides (Fig. 1l).

2.4. Lofoten Islands

The Lofoten Islands (Norway) mainly consist of Proterozoic gabbroic, dioritic, as well as associated olivine- and (ortho-)pyroxene-bearing monzonitic to granitic rocks. For convenience, the latter are grouped

Table 1

Overview of the textural occurrence of halogen-bearing minerals for the individual samples and references for additional information.

Locality	Sample	Literature description	Description used in this study	Halogen-bearing minerals			Previous studies on the used samples
				Apatite	Biotite	Amphibole	
Mont Saint-Hilaire	MSH17	Gabbro	Gabbro	x	x (1,3)	x (1,3)	Marks et al. (2012); Schilling et al. (2011a and b)
	MSH18	Gabbro	Gabbro	x	—	x (1,3)	
	MSH19	Diorite	Diorite	x	x (1,3)	—	
	MSH12	Diorite	Diorite	x	x (1,3)	x (1,3,4)	
	MSH75	Diorite	Diorite	x	x (1,3)	x (1,3,4)	
Ilímaussaq	GM1858	Augite syenite	Augite syenite	x	x (1,3)	x (1,2,3,4)	Marks and Markl (2001), Marks et al. (2004a, 2004b, 2007), Zirner et al. (submitted)
	GM1333	Augite syenite	Augite syenite	x	x (3)	x (2,3,4)	
	GM1332	Augite syenite	Augite syenite	x	x (2,3)	x (2,3,4)	
	GM1330	Augite syenite	Augite syenite	x	x (2,3)	x (2,3,4)	
	GM1857	Augite syenite	Augite syenite	x	x (2,3)	x (1,2,3,4)	
Ard.*	ARD17	Quartz monzonite	Quartz monzonite	x	x (1)	—	Not used in previous studies
	ARD16	Tonalite	Monzonite	x	x (1,3)	x (1)	
Lofoten Islands	GM349-3	Gabbro	Gabbro	x	x (4)	x (1,2,4)	Markl (2001), Markl and Frost (1999), Markl and Höhndorf (2003), Markl et al. (1998)
	GM500	Gabbro	Gabbro	x	x (1,4,5)	x (4)	
	GM448	Gabbro	Gabbro	x	x (3,4)	—	
	GM1082	Leucogabbro	Gabbro	x	x (3,4,5)	x (3,4,5)	
	GM1160	Leucogabbro	Gabbro	x	x (3,4)	—	
	GM1120	Ferrodiorite	Diorite	x	x (1,3,4)	—	
	GM384	Ferrodiorite	Diorite	x	x (1,3)	x (3)	
	GM451	Ferrodiorite	Diorite	x	x (3)	—	
	GM270	Charnockite	Mangeritic rock	x	x (3,4)	x (3,4)	
	GM1140	Mangerite	Mangeritic rock	x	x (3,4)	x (3,4)	
	GM378	Mangerite	Mangeritic rock	x	x (3,4)	x (3,4)	
	GM18	Mangerite	Mangeritic rock	x	x (3,4)	x (4)	
	GM393	Mangerite	Mangeritic rock	x	x (3,4,5)	x (1,3)	
	Kovd-10	Phoscorite	Phoscorite	x	x (1)	—	Not used in previous studies
Kola Peninsula	7/68	Carbonatite	Carbonatite	x	x (1)	—	
	205/274	Carbonatite	Carbonatite	x	x (1)	—	
	4/241	Carbonatite	Carbonatite	x	x (1)	—	
	1/552.5	Carbonatite	Carbonatite	x	x (1)	—	

Ard.* = Ardnamurchan; x = mineral observed within sample; — = mineral not observed within the sample; Textural distinction: 1 = discrete grain; 2 = replacing olivine; 3 = replacing Fe-Ti-oxide; 4 = replacing pyroxene; 5 = replacing hydrosilicate.

Table 2

Overview of the apatite, biotite and amphibole compositions present in the individual samples.

Locality	Sample	Description used in this study	Apatite group minerals	Biotite group minerals	Amphibole group minerals
Mont Saint-Hilaire	MSH17	Gabbro	Fluorapatite	Phlogopite	Karsutite
	MSH18	Gabbro	Fluorapatite	—	Karsutite
	MSH19	Diorite	Fluorapatite	Phlogopite	—
	MSH12	Diorite	Fluorapatite	Phlogopite	Karsutite
	MSH75	Diorite	Fluorapatite	Phlogopite	Karsutite
Ilímaussaq	GM1858	Augite syenite	Fluorapatite	Annite	Ferropargasite
	GM1333	Augite syenite	Fluorapatite	Annite	Ferropargasite to ferro-edenite
	GM1332	Augite syenite	Fluorapatite	Annite	Ferropargasite to ferro-edenite
	GM1330	Augite syenite	Fluorapatite	Annite	Ferropargasite to ferro-edenite
	GM1857	Augite syenite	Fluorapatite	Annite	Ferropargasite to ferro-edenite
Ard.*	ARD17	Quartz monzonite	Fluorapatite	Phlogopite	—
	ARD16	Monzonite	Fluorapatite	Phlogopite	Ferro-edenite
Lofoten Islands	GM349-3	Gabbro	Hydroxylapatite	Phlogopite	Pargasite
	GM500	Gabbro	Fluorapatite	Phlogopite	Pargasite to edenite
	GM448	Gabbro	Fluorapatite	Phlogopite	—
	GM1082	Gabbro	Fluor-hydroxylapatite	Phlogopite	Pargasite
	GM1160	Gabbro	Fluorapatite	Phlogopite	—
	GM1120	Diorite	Fluorapatite	Phlogopite	—
	GM384	Diorite	Fluorapatite	Annite	Edenite
	GM451	Diorite	Fluorapatite	Phlogopite	—
	GM270	Mangeritic rock	Fluorapatite	Phlogopite	Pargasite to edenite
	GM1140	Mangeritic rock	Fluorapatite	Phlogopite	Pargasite
	GM378	Mangeritic rock	Fluorapatite	Annite	Ferropargasite to ferro-edenite
	GM18	Mangeritic rock	Fluorapatite	Annite	Ferro-edenite
	GM393	Mangeritic rock	Fluorapatite	Annite	Ferro-edenite
	Kovd-10	Phoscorite	Hydroxylapatite	Tetraferriphlogopite	—
Kola Peninsula	7/68	Carbonatite	Hydroxylapatite	Phlogopite	—
	205/274	Carbonatite	Hydroxylapatite	Phlogopite	—
	4/241	Carbonatite	Hydroxylapatite	Phlogopite	—
	1/552.5	Carbonatite	Hydroxylapatite	Phlogopite	—

Ard.* = Ardnamurchan; — = mineral not observed within the sample.

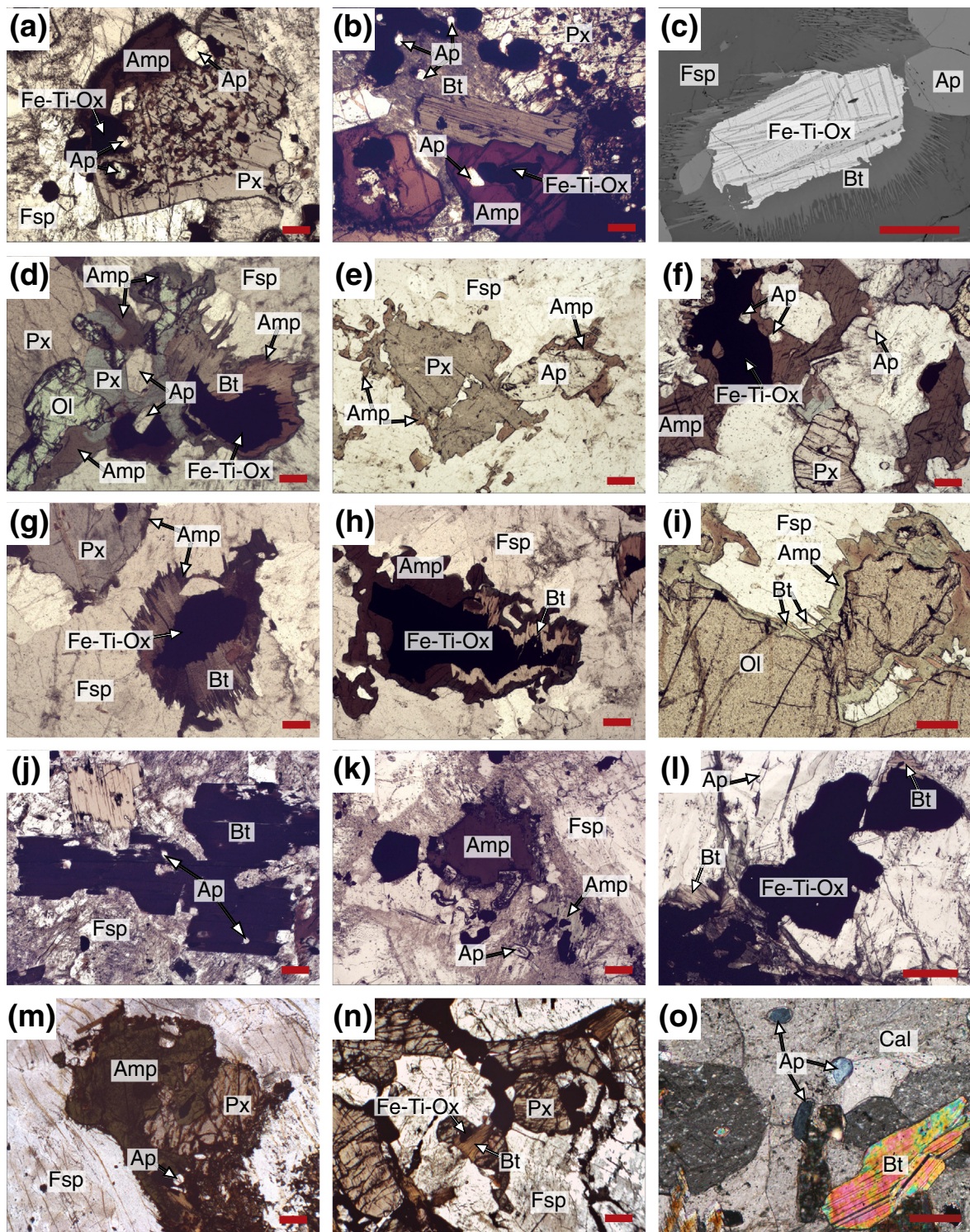


Fig. 1. Photomicrographs (scale: red bar = 200 µm) of apatite, biotite and amphibole textures. Sample represented (a) MSH12; (b) MSH75; (c) MSH119; (d) GM1330; (e) GM1332; (f) GM1858; (g) GM1330; (h) GM1332; (i) ARD17; (j) ARD16; (k) ARD16; (l) GM18; (n) GM1160; (o) 4/241. Abbreviations: Amp = amphibole; Ap = apatite; Bt = biotite; Cal = calcite; Fe-Ti-Ox = Fe-Ti oxides (ilmenite or magnetite); Fsp = feldspar; Ol = olivine; Px = pyroxene. (For interpretation of the references to color in this figure legend, the reader is referred to the web version of this article.)

together and are referred to as mangeritic rocks in the following. This rock suite originated from multistage fractionation of mantle-derived melts combined with the assimilation of lower crustal rocks (e.g., Markl and Frost, 1999; Markl, 2001; Markl and Höhndorf, 2003; Corfu, 2004).

The investigated gabbroic (GM349-3, 448, 500, 1082 and 1160), dioritic (GM384, 451 and 1120) and mangeritic rocks (GM18, 270,

378, 393 and 1140) contain ternary feldspar, clino- and orthopyroxene, Fe-Ti oxides, ± olivine, apatite, ± amphibole, ± biotite, pyrrhotite, ± zircon. Apatite (50–300 µm) occurs in all rock samples as sub- to euhedral inclusions in feldspar, pyroxenes and Fe-Ti oxides or along grain boundaries between these minerals (Fig. 1m and n). All samples contain small amounts of fine-grained and texturally late biotite and/

or amphibole replacing pyroxenes and Fe–Ti oxides. A few samples additionally contain up to 1 mm large subhedral amphibole (GM349–3 and 393) or biotite (GM384, 500 and 1120).

2.5. Kola Peninsula

The Kola Peninsula (Russia) was intruded in Devonian times by several rift-related alkaline to carbonatitic complexes that are formed from mantle-derived melts (e.g., Marty et al., 1998; Arzamastsev et al., 2001; Wall and Zaitsev, 2004; Zaitsev et al., 2014).

Calcite carbonatite samples from Kovdor (1/522.5, 4/241 and 7/68) and Vuoriyarvi (205/274) drill holes which cut the main carbonatite stocks of the massifs, contain calcite, magnetite, apatite, biotite (phlogopite), and ± tremolite. Euhedral to subhedral apatite (100–300 µm) and 1–5 mm large phlogopites are common phases. A sample from Kovdor (KOVD-10) collected from the open pit, belongs to the calcite–forsterite–magnetite phoscorite variety (Krasnova et al., 2004) with tetraferriphlogopite (Fig. 1o).

2.6. Analytical methods

The analytical data was collected at the Mathematisch-Naturwissenschaftliche Fakultät, Fachbereich Geowissenschaften, Eberhard Karls Universität Tübingen (Germany). Electron microprobe analyses utilized a JEOL 8900 electron microprobe in the wavelength-dispersive mode (WDS). For apatite analyses we applied an acceleration voltage of 15 kV, a beam current of 10 nA and a beam diameter of 10 µm. These operating conditions are very similar to those used by Teiber et al. (2014) and Wang et al. (2014b) and were chosen to prohibit significant time-dependent variations in halogen X-ray counts, which are partly caused by different crystallographic orientation of the apatite relative to the electron beam (see details in Goldoff et al., 2012; Stock et al., 2015; Stormer et al., 1993).

For biotite and amphibole analyses we used an acceleration voltage of 15 kV, a beam current of 20 nA and varying beam diameters between 2 and 10 µm. The raw data were processed using the JEOL integrated φpz and ZAF corrections for hydroxyl-bearing silicates and apatite, respectively (Armstrong, 1991). More details (e.g., detection limits, standard deviations and used standard materials) are given in the electronic supplement (Table A.1).

Analyses for Br were acquired using a benchtop TXRF system (S2 PICOFOX) from Bruker AXS Microanalysis GmbH equipped with a Mo-tube operating at 50 kV and 600 µA. Handpicked separates of apatite, biotite and amphibole were cleaned with MilliQ water and then milled to a fine powdered with an agate mortar. Between 1 and 5 mg of these powders were dispersed in a mixture of 1 ml TritonX-100 solution (1 vol.%) with Se as an internal standard. After homogenization, several 10 µl aliquots of suspension were pipetted onto polished quartz-glass disks and dried on a heating plate at 70 °C. Each dried sample was then analyzed for 1000 s and the raw data were fitted using the Spectra software 6.2.0.0 (Bruker AXS Microanalysis GmbH). Pile-up corrections were applied for Ca, P and Fe (apatites) and Fe, Ti, K and Ca (biotite and amphibole). To ensure accuracy of the Br determinations, we periodically re-analyzed several apatite samples previously characterized by Marks et al. (2012).

3. Results

The abundances of F and Cl in apatite, biotite and amphibole are reported as molar fractions of F ($X_F = \text{molar } F / (F + Cl + OH)$) and Cl ($X_{Cl} = \text{molar } Cl / (F + Cl + OH)$), based on the assumption of a fully occupied OH-site. A general overview of the results is given in Table 3 showing median, mean, maximum and minimum values of X_F and X_{Cl} , as well as the respective F-, Cl- (wt.%) and Br-contents (µg/g) for each mineral in each sample. Halogen data and major and minor element compositions of apatite, biotite and amphibole including textural

information for the analytical locations are given in the supplementary data files (Tables A.2, A.3 and A.4). The halogen data are illustrated in Fig. 2–4, with the data for each locality are arranged from left to right by decreasing #Mg values (molar Mg/(Fe + Mg)) of either available whole rock (Ilímaussaq and Lofoten Islands samples), olivine (Mont Saint-Hilaire samples) or magmatic biotite (Kola Peninsula samples) compositions. To investigate potential crystal chemical effects on the incorporation of F and Cl in biotite and amphibole, we use the molar fraction of Mg relative to other octahedral cations ($X_{Mg} = Mg / (Mg + Fe + Mn + Ti + Al^{VI})$) and a modified X_{Fe}^* -value ($X_{Fe}^* = (Fe + Al^{VI}) / (Fe + Mg + Al^{VI})$) as introduced by Zhu and Sverjensky (1992).

3.1. Apatite

Sub- to euhedral apatite occurs in all samples as an early magmatic phase in various textural relationships (Fig. 1). In gabbroic rocks, apatite shows highly variable X_F ranging to quite low values (0.18 to 0.75). The low values and variability is less for apatite from carbonatitic (0.33 to 0.58), dioritic (0.59 to 0.90) and monzonitic rocks (0.57 to 0.90) and reaches the highest values in apatite from mangeritic (0.71 to 1.00) and syenitic rocks (0.78 to 1.00; Table 3; Fig. 2a).

Relatively high X_{Cl} values (up to 0.18) are present in apatite from gabbroic, dioritic, monzonitic and some mangeritic rocks (Table 3; Fig. 3a). The lowest X_{Cl} values (mostly <0.01) occur in apatite from syenitic and carbonatitic rocks. Among the syenitic samples, the most primitive one (GM1858) shows the highest X_{Cl} values. There is no clear relationship between F and Cl contents of apatite show no clear dependence on their textural relations.

Mean Br contents for most apatites vary from below detection limit (b.d.l.) of around 0.3 µg/g to 2.0 µg/g (Table 3; Fig. 4a). Higher Br concentrations were found in apatite from monzonite ARD16 (2.3 µg/g) and quartz-monzonite ARD17 (3.7 µg/g), and from three gabbroic rocks (MSH17, MSH18 and GM1082) reaching (3.4, 2.9 and 9.9 µg/g, respectively). A general correlation between mean/median Cl and Br contents among apatites is not obvious, except for the syenitic samples from Ilímaussaq, where mean Cl decreases with an increasing degree of differentiation and Br contents remain constant (Table 3), resulting in a continuous decrease in the Cl/Br mass ratios (Fig. 4b).

3.2. Biotite

Fluorine abundances in biotites are highly variable ranging from below the detection limit (in some gabbroic rocks) up to 0.67 X_F in a mangeritic rock, with no clear relationship with respect to rock type (Table 3; Fig. 2b). Within a given locality, however, the biotites X_F generally correlate with the F systematics observed for apatites. For example, in mangeritic rocks from the Lofoten Islands F-rich biotites replacing precursor pyroxene or Fe–Ti oxides occur together with F-rich apatites and vice versa. In many samples, the total range in X_F is relatively small (e.g., Lofoten samples) even if biotites in a sample occur as both discrete grains (presumably magmatic) and as (late-stage) replacements of precursor minerals (Fig. 2b). In other samples biotites show a larger range of X_F (e.g., Mont Saint-Hilaire), although both textural occurrences of biotite (discrete primary and secondary phases) in these samples cover a very similar range in X_F . The largest spreads of X_F are shown in biotites from syenitic rocks of the Ilímaussaq complex, where X_F in biotites may vary by two orders of magnitude in a given sample (Fig. 2b). Importantly, the different textural occurrences of biotite in these samples contain different amounts of F: biotites replacing olivine show the highest X_F values (up to 0.35) and those replacing Fe–Ti oxides have lower values (mostly well below 0.1). In addition, biotites from these samples show a positive correlation between X_F and X_{Mg} , with biotites replacing olivines showing higher X_{Mg} values than those replacing Fe–Ti oxides (Fig. 5a). This is consistent with the so-called Fe–F or Mg–Cl avoidance rule (Muñoz, 1984; Mason, 1992; Léger et al., 1996;

Table 3

Fluorine, chlorine and bromine contents of apatite, biotite and amphibole given as in [wt.%; µg/g] and molar fraction for F [XF] and Cl [XCl].

			Apatite						Biotite						Amphibole									
			EMPA			TXRF			EMPA			TXRF			EMPA			TXRF						
			wt.%		molar		µg/g		wt.%		molar		µg/g		wt.%		molar		µg/g					
			Cl	F	XCl	XF	n	Br	n	Cl	F	XCl	XF	n	Br	n	Cl	F	XCl	XF	n	Br	n	
Mont Saint Hilaire	Gabbro	MSH17	Mean	0.32 ± 0.07	2.17 ± 0.11	0.047 ± 0.010	0.593 ± 0.030	41	3.4 ± 0.1	9	0.05 ± 0.02	0.17 ± 0.06	0.003 ± 0.001	0.020 ± 0.006	21	4.0 ± 0.6	6	0.02 ± 0.01	0.14 ± 0.04	0.003 ± 0.001	0.032 ± 0.009	31	0.5 ± 0.2	
			Median	0.31	2.16	0.045	0.593		0.04		0.02	0.19	0.003	0.021		0.02		0.13	0.003	0.031				
			Min	0.24	1.98	0.035	0.542		0.03		0.07	0.002	0.002	0.008		0.01		0.05	0.001	0.011				
			Max	0.47	2.37	0.069	0.643		0.09		0.29	0.006	0.006	0.034		0.05		0.23	0.006	0.053				
			MSH18	Mean	0.37 ± 0.07	2.18 ± 0.09	0.054 ± 0.010	0.590 ± 0.024	49	2.9 ± 0.3	8					X			0.03 ± 0.01	0.17 ± 0.05	0.004 ± 0.001	0.039 ± 0.011	55	0.8 ± 0.3
		MSH119	Median	0.36	2.19	0.053	0.596									0.01		0.05	0.001	0.011				
			Min	0.27	1.98	0.039	0.536									0.03		0.17	0.004	0.039				
			Max	0.51	2.35	0.075	0.636									0.01		0.03	0.001	0.007				
			Diorite	Mean	0.25 ± 0.07	2.99 ± 0.18	0.036 ± 0.010	0.813 ± 0.047	33	0.9 ± 0.2	8	0.06 ± 0.03	1.26 ± 0.25	0.002 ± 0.002	0.145 ± 0.028	51	1.5 ± 0.3	5				X		
			Median	0.24	3.03	0.036	0.820					0.05	1.27	0.003	0.146									
Ilímaussaq	Augite syenite	GM1858	Min	0.15	2.65	0.022	0.725				0.03	0.81	0.002	0.095										
			Max	0.43	3.33	0.063	0.896				0.12	1.83	0.007	0.209										
			Mean	0.23 ± 0.06	2.84 ± 0.15	0.033 ± 0.009	0.772 ± 0.040	54	0.7 ± 0.2	10	0.07 ± 0.02	1.09 ± 0.17	0.004 ± 0.001	0.126 ± 0.019	47	1.5 ± 0.3	8	0.05 ± 0.01	0.74 ± 0.27	0.006 ± 0.002	0.172 ± 0.063	53	0.4 ± 0.1	
			Median	0.21	2.89	0.031	0.785				0.06	1.04	0.004	0.120				0.05	0.61	0.006	0.143			
			Min	0.17	2.57	0.024	0.698				0.02	0.87	0.001	0.101				0.03	0.49	0.004	0.113			
		MSH12	Max	0.46	3.09	0.066	0.837				0.13	1.83	0.008	0.211				0.10	1.38	0.012	0.322			
			Mean	0.19 ± 0.05	2.63 ± 0.13	0.028 ± 0.007	0.713 ± 0.036	25	0.9 ± 0.2	7	0.05 ± 0.01	0.58 ± 0.24	0.003 ± 0.001	0.070 ± 0.028	42	2.0 ± 0.4	6	0.03 ± 0.01	0.27 ± 0.06	0.004 ± 0.002	0.064 ± 0.015	27	1.0 ± 0.1	
			Median	0.18	2.63	0.027	0.714				0.05	0.50	0.003	0.059				0.03	0.28	0.004	0.065			
			Min	0.12	2.39	0.018	0.649				0.03	0.27	0.002	0.033				0.02	0.15	0.002	0.036			
			Max	0.31	2.85	0.045	0.778				0.08	1.26	0.005	0.148				0.08	0.41	0.010	0.095			
Ilímaussaq	Augite syenite	GM1858	Mean	0.06 ± 0.01	3.28 ± 0.14	0.008 ± 0.002	0.876 ± 0.036	54	1.0 ± 0.2	4	0.06 ± 0.01	1.18 ± 0.26	0.004 ± 0.001	0.143 ± 0.031	15	7.7 ± 2.6	6	0.09 ± 0.02	0.96 ± 0.11	0.012 ± 0.002	0.234 ± 0.028	45	n.q.	
			Median	0.06	3.27	0.008	0.870				0.07	1.22	0.004	0.148				0.09	0.95	0.012	0.232			
			Min	0.03	2.99	0.004	0.798				0.04	0.53	0.003	0.066				0.07	0.77	0.009	0.186			
			Max	0.09	3.63	0.013	0.972				0.08	1.50	0.005	0.182				0.13	1.25	0.018	0.303			
			Mean	0.020 ± 0.01	3.34 ± 0.01	0.002 ± 0.001	0.885 ± 0.044	41	1.5 ± 0.3	4	0.06 ± 0.03	0.32 ± 0.23	0.004 ± 0.002	0.041 ± 0.029	27	n.a.		0.08 ± 0.02	1.00 ± 0.40	0.010 ± 0.002	0.248 ± 0.097	41	n.q.	
		GM1333	Median	0.02	3.37	0.002	0.897				0.05	0.29	0.003	0.036				0.08	0.85	0.010	0.213			
			Min	b.d.l.	2.90	b.d.l.	0.775				0.03	b.d.l.	0.002	0.000				0.02	0.45	0.003	0.116			
			Max	0.03	3.67	0.004	0.965				0.11	0.87	0.008	0.109				0.12	1.68	0.016	0.414			
			Mean	0.01 ± 0.01	3.36 ± 0.20	0.001 ± 0.001	0.904 ± 0.051	43	n.a.		0.05 ± 0.01	0.78 ± 0.85	0.003 ± 0.001	0.098 ± 0.106	23	3.0 ± 0.9	2	0.06 ± 0.02	1.26 ± 0.50	0.009 ± 0.003	0.317 ± 0.123	50	n.q.	
			Median	0.01	3.32	0.001	0.905				0.05	0.35	0.003	0.044				0.06	1.24	0.008	0.310			
Ilímaussaq	Augite syenite	GM1332	Min	b.d.l.	3.03	b.d.l.	0.810				0.02	b.d.l.	0.002	0.000				0.03	0.45	0.005	0.116			
			Max	0.02	3.80	0.003	1.009				0.07	2.68	0.004	0.334				0.10	2.21	0.014	0.546			
			Mean	0.01 ± 0.01	3.39 ± 0.15	0.001 ± 0.001	0.911 ± 0.044	40	0.8 ± 0.1	4	0.05 ± 0.01	1.17 ± 0.75	0.003 ± 0.001	0.148 ± 0.093	31	1.5 ± 0.2	6	0.07 ± 0.02	0.94 ± 0.33	0.009 ± 0.002	0.237 ± 0.082	44	b.d.l.	
			Median	0.01	3.36	0.001	0.902				0.05	0.85	0.003	0.107				0.07	0.84	0.009	0.209			
			Min	b.d.l.	3.05	b.d.l.	0.825				0.03	0.24	0.002	0.031				0.03	0.53	0.004	0.136			
		GM1330	Max	0.03	3.70	0.004	0.994				0.08	2.83	0.005	0.353				0.10	1.73	0.013	0.428			
			Mean	0.01 ± 0.01	3.39 ± 0.15	0.001 ± 0.001	0.907 ± 0.031	18	1.2 ± 0.1	5	0.03 ± 0.01	0.37 ± 0.41	0.002 ± 0.001	0.048 ± 0.052	25	0.7 ± 0.3	5	0.06 ± 0.02	0.99 ± 0.35	0.009 ± 0.003	0.254 ± 0.087	37	b.d.l.	
			Median	0.00	3.41	0.001	0.914				0.03	0.22	0.002	0.028				0.05	0.93	0.007	0.237			
			Min	b.d.l.	3.10	b.d.l.	0.864				0.02	b.d.l.	0.001	0.000				0.03	0.50	0.004	0.129			
			Max	0.02	3.61	0.003	0.960				0.05	1.35	0.004	0.173				0.10	1.73	0.014	0.435			

Ardnamurchan	Monzonite	ARD17	Mean	1.00 ± 0.20	2.45 ± 0.20	0.143 ± 0.022	0.660 ± 0.052	50	3.7 ± 0.2	3	0.26 ± 0.10	1.27 ± 0.16	0.016 ± 0.006	0.151 ± 0.019	55	0.6 ± 0.1	3	X						
			Median	1.05	2.40	0.151	0.648				0.27	1.28	0.017	0.152										
			Min	0.68	2.13	0.098	0.575				0.10	0.90	0.006	0.108										
			Max	1.25	2.82	0.180	0.756				0.42	1.54	0.027	0.183										
		ARD16	Mean	0.44 ± 0.10	2.83 ± 0.24	0.064 ± 0.015	0.760 ± 0.064	75	2.3 ± 0.1	3	0.51 ± 0.06	1.08 ± 0.63	0.033 ± 0.004	0.129 ± 0.075	12	n.a.	0.41 ± 0.07	1.61 ± 0.16	0.053 ± 0.009	0.270 ± 0.038	50	b.d.l.	3	
			Median	0.43	2.84	0.061	0.761				0.51	0.91	0.032	0.109			0.40	1.62	0.052	0.392				
			Min	0.28	2.10	0.040	0.572				0.44	0.31	0.028	0.037			0.21	1.12	0.027	0.389				
			Max	0.82	3.38	0.120	0.902				0.62	2.04	0.040	0.245			0.60	2.07	0.078	0.497				
Lofoten Islands	Gabbro	GM349-3	Mean	0.55 ± 0.28	0.92 ± 0.22	0.078 ± 0.039	0.243 ± 0.058	15	n.a.		0.03 ± 0.01	b.d.l.	0.002 ± 0.001	b.d.l.	20	n.a.	0.02 ± 0.002	b.d.l.	0.002 ± 0.002	b.d.l.	23	n.a.		
			Median	0.64	0.84	0.090	0.221				0.02	b.d.l.	0.001	b.d.l.			0.02	b.d.l.	0.002	b.d.l.				
			Min	0.12	0.68	0.017	0.182				0.02	b.d.l.	0.001	b.d.l.			b.d.l.	b.d.l.	b.d.l.	b.d.l.				
			Max	1.16	1.36	0.164	0.359				0.04	b.d.l.	0.003	b.d.l.			0.04	b.d.l.	0.005	b.d.l.				
		GM500	Mean	0.36 ± 0.03	2.66 ± 0.11	0.050 ± 0.005	0.700 ± 0.029	14	n.a.		0.17 ± 0.01	0.34 ± 0.04	0.011 ± 0.001	0.041 ± 0.005	18	n.a.	0.22 ± 0.02	0.06 ± 0.04	0.027 ± 0.005	0.014	10	n.a.		
			Median	0.35	2.64	0.049	0.691				0.17	0.34	0.011	0.041			0.20	0.07	0.026	0.017				
			Min	0.32	2.51	0.045	0.665				0.15	0.26	0.009	0.031			0.17	b.d.l.	0.021	b.d.l.				
			Max	0.44	2.85	0.062	0.752				0.19	0.40	0.012	0.047			0.27	0.10	0.035	0.023				
		GM448	Mean	0.34 ± 0.04	2.49 ± 0.10	0.048 ± 0.006	0.655 ± 0.026	15	n.a.		0.07 ± 0.01	0.28 ± 0.03	0.005 ± 0.001	0.032 ± 0.003	23	n.a.					X			
			Median	0.33	2.50	0.047	0.655				0.08	0.28	0.005	0.032										
			Min	0.26	2.28	0.036	0.600				0.04	0.23	0.003	0.026										
			Max	0.43	2.69	0.060	0.704				0.10	0.35	0.006	0.041										
Lofoten Islands	Gabbro	GM1082	Mean	0.35 ± 0.08	1.77 ± 0.08	0.051 ± 0.012	0.473 ± 0.023	21	9.9 ± 0.5	4	0.08 ± 0.02	b.d.l.	0.005 ± 0.001	b.d.l.	20	n.a.	0.09 ± 0.02	b.d.l.	0.012 ± 0.003	b.d.l.	9	n.a.		
			Median	0.35	1.75	0.050	0.470				0.08	b.d.l.	0.005	b.d.l.			0.10	b.d.l.	0.013	b.d.l.				
			Min	0.27	1.56	0.038	0.416				0.07	b.d.l.	0.004	b.d.l.			0.04	b.d.l.	0.005	b.d.l.				
			Max	0.54	1.89	0.078	0.509				0.12	b.d.l.	0.008	b.d.l.			0.13	b.d.l.	0.016	b.d.l.				
		GM1160	Mean	0.25 ± 0.01	2.42 ± 0.08	0.035 ± 0.002	0.647 ± 0.022	17	1.4 ± 0.1	4	0.08 ± 0.01	0.22 ± 0.03	0.005 ± 0.004	0.026 ± 0.026	26	n.a.					X			
			Median	0.25	2.41	0.035	0.646				0.07	0.22	0.005	0.026										
			Min	0.22	2.24	0.032	0.601				0.06	0.15	0.004	0.018										
			Max	0.27	2.54	0.039	0.681				0.11	0.27	0.007	0.032										
Diorite	GM1120	Mean	0.21 ± 0.02	2.63 ± 0.10	0.030 ± 0.003	0.694 ± 0.025	15	n.a.			0.04 ± 0.01	0.33 ± 0.03	0.003 ± 0.001	0.039 ± 0.005	25	n.a.					X			
			Median	0.22	2.62	0.031	0.690				0.05	0.34	0.003	0.040										
			Min	0.16	2.46	0.034	0.653				0.03	0.25	0.002	0.030										
			Max	0.24	2.87	0.023	0.757				0.06	0.40	0.003	0.049										
		GM384	Mean	0.12 ± 0.03	2.68 ± 0.12	0.017 ± 0.004	0.708 ± 0.030	4	1.4 ± 0.2	4	0.08 ± 0.04	0.28 ± 0.03	0.005 ± 0.003	0.034 ± 0.003	15	n.a.	0.03 ± 0.02	0.05 ± 0.07	0.004 ± 0.003	0.012 ± 0.017	2	n.a.		
			Median	0.11	2.65	0.016	0.708				0.09	0.28	0.006	0.034			0.03	0.05	0.004	0.012				
			Min	0.08	2.40	0.011	0.642				0.02	0.23	0.001	0.027			0.01	b.d.l.	0.001	b.d.l.				
			Max	0.17	2.83	0.024	0.749				0.13	0.33	0.008	0.040			0.04	0.10	0.006	0.024				
		GM451	Mean	0.40 ± 0.05	2.50 ± 0.14	0.056 ± 0.007	0.660 ± 0.036	16	n.a.		0.09 ± 0.03	0.27 ± 0.11	0.006 ± 0.002	0.031 ± 0.013	11	n.a.	X							
			Median	0.40	2.49	0.058	0.661				0.11	0.24	0.006	0.027										
			Min	0.29	2.23	0.041	0.587				0.04	0.09	0.002	0.011										
			Max	0.47	2.72	0.066	0.714				0.11	0.44	0.007	0.051										
Mangeritic rock	GM270	Mean	0.05 ± 0.01	3.52 ± 0.18	0.006 ± 0.001	0.942 ± 0.044	15	n.a.			0.10 ± 0.03	4.47 ± 0.54	0.006 ± 0.002	0.514 ± 0.059	13	n.a.	0.17 ± 0.06	1.96 ± 0.54	0.022 ± 0.059	0.460 ± 0.18	19	n.a.		
			Median	0.05	3.55	0.007	0.955				0.10	4.36	0.007	0.500			0.20	1.97	0.025	0.461				
			Min	0.03	3.27	0.004	0.879				0.06	3.57	0.003	0.423			0.09	1.57	0.011	0.366				
			Max	0.06	3.77	0.009	0.998				0.17	5.80	0.011	0.663			0.27	2.22	0.034	0.529				
		GM1140	Mean	0.22 ± 0.02	3.11 ± 0.10	0.032 ± 0.003	0.826 ± 0.026	19	n.a.		0.33 ± 0.03	0.85 ± 0.08	0.021 ± 0.002	0.101 ± 0.009	14	n.a.	0.31 ± 0.01	0.37 ± 0.08	0.038 ± 0.007	0.087 ± 0.015	5	n.a.		
			Median	0.22	3.11	0.032	0.826				0.33	0.85	0.021	0.101			0.31	0.37	0.038	0.087				
			Min	0.19	2.98	0.028	0.789				0.28	0.80	0.019	0.099			0.30	0.35	0.037	0.086				
			Max	0.27	3.48	0.040	0.938				0.38	0.92	0.027	0.127			0.34	0.42	0.045	0.104				

(continued on next page)

Table 3 (continued)

		Apatite								Biotite								Amphibole															
		EMPA				TXRF				EMPA				TXRF				EMPA				TXRF											
		wt.%		molar		μg/g		wt.%		molar		μg/g		wt.%		molar		μg/g		wt.%		molar		μg/g									
		Cl	F	XCl	XF	n	Br	n	Cl	F	XCl	XF	n	Br	n	Cl	F	XCl	XF	n	Br	n	Cl	F	XCl	XF	n	Br	n				
Kola Peninsula	Phosc.*	GM378	Median	0.23	3.09	0.032	0.820		0.33	0.84	0.021	0.100				0.31	0.37	0.038	0.088														
			Min	0.00	b.d.l.	0.026	0.783		0.29	0.71	0.018	0.084				0.29	0.27	0.036	0.064														
			Max	0.26	3.29	0.037	0.876		0.41	0.98	0.026	0.116				0.32	0.45	0.040	0.105														
			Mean	0.16 ± 0.08	3.00 ±	0.023 ±	0.802 ±	16	1.7 ± 4	0.30 ±	0.32 ±	0.020 ±	0.040 ±	12	n.a.		0.28 ±	0.09 ±	0.037 ±	0.021 ±	11	n.a.											
						0.14	0.012	0.036		0.1	0.12	0.03	0.008				0.20	0.03	0.027	0.008													
		GM18	Median	0.14	3.00	0.020	0.798		0.29	0.32	0.019	0.039				0.26	0.09	0.034	0.023														
			Min	0.08	2.78	0.012	0.742		0.02	0.28	0.001	0.034				0.02	0.04	0.003	0.010														
			Max	0.37	3.43	0.053	0.907		0.52	0.39	0.034	0.049				0.65	0.13	0.087	0.030														
			Mean	0.06 ± 0.01	2.92 ±	0.008 ±	0.779 ±	17	1.6 ± 4	0.23 ±	0.06 ±	0.015 ±	0.007 ±	28	n.a.		0.35 ±	b.d.l.	0.047 ±	b.d.l.	7	n.a.											
						0.18	0.002	0.049		0.1	0.07	0.03	0.005				0.02																
Kola Peninsula	Kovd-10	GM393	Median	0.06	2.88	0.008	0.764		0.19	0.05	0.013	0.007				0.36	b.d.l.	0.047	b.d.l.														
			Min	0.03	2.66	0.004	0.709		0.17	b.d.l.	0.011	b.d.l.				0.31	b.d.l.	0.040	b.d.l.														
			Max	0.08	3.29	0.012	0.882		0.36	0.11	0.024	0.014				0.38	b.d.l.	0.049	b.d.l.														
			Mean	0.01 ± 0.02	3.27 ±	0.002 ±	0.871 ±	17	0.9 ± 4	0.18 ±	0.43 ±	0.012 ±	0.054 ±	17	n.a.		0.45 ±	0.21 ±	0.060 ±	0.052	17	n.a.											
						0.15	0.002	0.038		0.1	0.17	0.13	0.011				0.14	0.04	0.019														
		7/68	Median	0.01	3.29	0.001	0.875		0.10	0.42	0.007	0.052				0.50	0.22	0.066	0.054														
			Min	b.d.l.	3.00	b.d.l.	0.800		0.05	0.29	0.003	0.037				0.18	0.14	0.024	0.034														
			Max	0.06	3.46	0.008	0.922		0.46	0.66	0.030	0.085				0.59	0.28	0.079	0.069														
			Mean	0.01 ±	1.51 ±	0.001 ±	0.399 ±	17	0.9 ± 4	0.01 ±	0.11 ±	0.001 ±	0.012 ±	18		1.3 ± 4					X												
					0.004	0.11	0.001	0.029		0.4	0.01	0.05	0.001				0.4																
Carbonatite	205/274	4/241	Median	0.01	1.47	0.001	0.390		0.01	0.10	0.001	0.011				b.d.l.					X												
			Min	b.d.l.	1.35	b.d.l.	0.358		b.d.l.	0.04	b.d.l.	0.004																					
			Max	0.01	1.75	0.002	0.465		0.04	0.21	0.002	0.024																					
			Mean	0.01 ±	1.47 ±	0.001 ±	0.387 ±	17	0.9 ± 4	0.01 ±	0.27 ±	0.000 ±	0.030 ±	18																			
					0.003	0.05	0.001	0.014		0.4	0.01	0.04	0.001																				
		1/552.5	Median	0.01	1.48	0.001	0.388		b.d.l.	0.27	b.d.l.	0.030																					
			Min	b.d.l.	1.38	b.d.l.	0.363		b.d.l.	0.19	b.d.l.	0.022																					
			Max	0.02	1.58	0.002	0.414		0.03	0.33	0.002	0.037																					
			Mean	0.01 ± 0.01	1.83 ±	0.001 ±	0.486 ±	22	b.d.l.	0.01 ±	0.51 ±	0.000 ±	0.057 ±	18		1.1 ± 4					X												
					0.13	0.001	0.035		0.1	0.01	0.020	0.014																					
Kola Peninsula	1/552.5	4/241	Median	0.01	1.80	0.001	0.479		0.01	0.50	0.000	0.055																					
			Min	b.d.l.	1.65	b.d.l.	0.443		b.d.l.	0.19	b.d.l.	0.021																					
			Max	0.02	2.16	0.003	0.583		0.01	0.74	0.001	0.083																					
			Mean	0.01 ± 0.01	1.47 ±	0.001 ±	0.389 ±	17	1.1 ± 4	0.01 ±	0.16 ±	0.000 ±	0.018 ±	190.9	4						X												
					0.09	0.001	0.025		0.1	0.01	0.04	0.000																					
		1/552.5	Median	0.01	1.49	0.002	0.394		0.01	0.18	0.000	0.020																					
			Min	b.d.l.	1.31	b.d.l.	0.344		b.d.l.	0.07	b.d.l.	0.008																					
			Max	0.02	1.63	0.002	0.435		0.02	0.22	0.001	0.024																					
			Mean	0.03 ± 0.01	1.40 ±	0.004 ±	0.373 ±	8	0.9 ± 4	0.02 ±	0.09 ±	0.001 ±	0.009 ±	14		b.d.l.	4				X												
					0.10	0.001	0.028		0.6	0.01	0.04	0.000																					

EPMA = electron microprobe microanalyzer; TXRF = total reflection X-ray fluorescence; XF = molar F/(F + Cl + OH); XCl = molar Cl/(F + Cl + OH); n = number of analyses; n.a. = not analyzed; n.q. = not quantifiable; b.d.l. = below detection limit; X = mineral not observed.

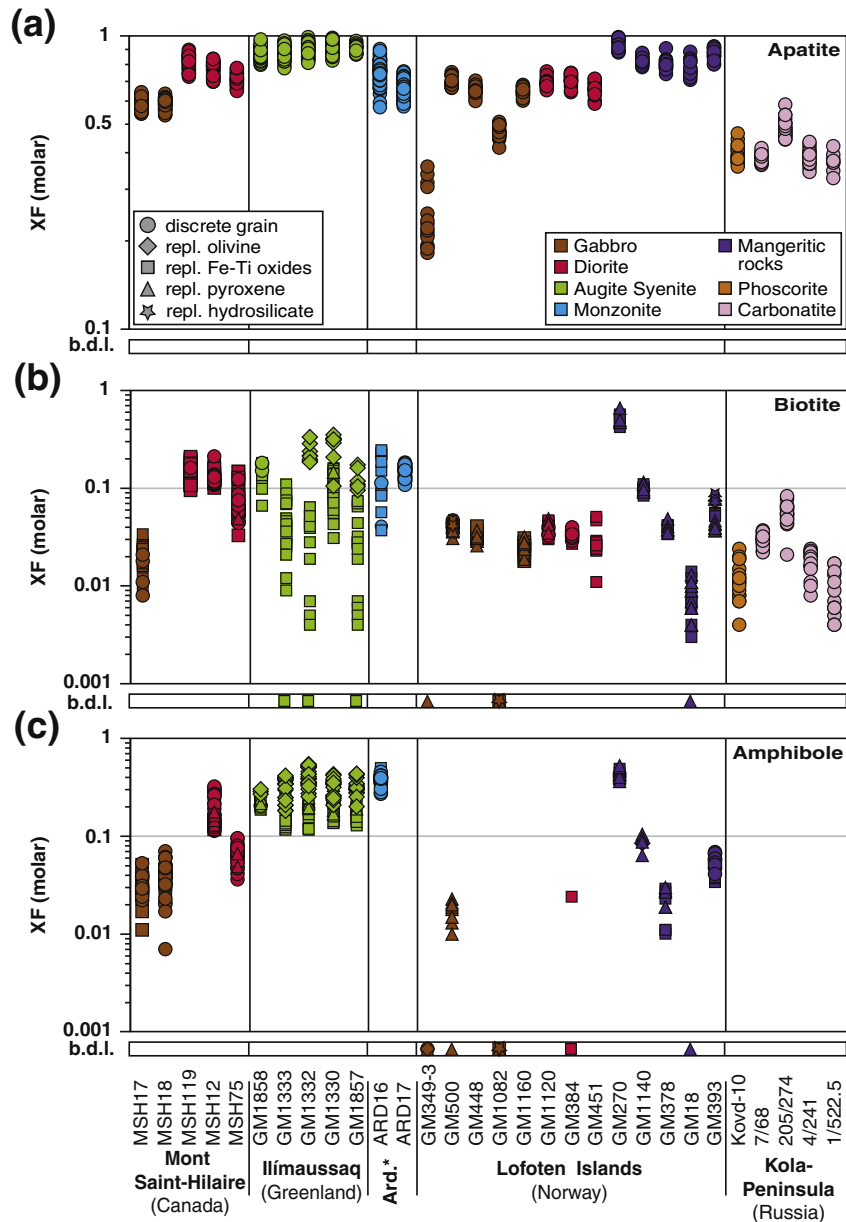


Fig. 2. Molar fraction of F (X_F) in (a) apatite, (b) biotite and (c) amphibole. From left to right, samples are grouped by locality and by increasing degree of differentiation. Ard.* = Ardnamurchan (Scotland).

Zhang et al., 2012). Although texturally similar, biotites from Mont Saint-Hilaire and the Lofoten Islands samples do not show such obvious systematics, mostly because of the much smaller variability in X_{Mg} .

The X_{Cl} values in biotites are usually one to two orders of magnitude lower compared to X_F . They are highest in monzonitic and some mangeritic rocks (up to 0.04), intermediate in gabbroic, dioritic and syenitic rocks (between about 0.001 and 0.01) and lowest (<0.01) in carbonatitic rocks (Table 3; Fig. 3b). A correlation of X_{Cl} values with the textural occurrence or the major element composition of biotites (X_{Mg}) is generally not observed.

Most biotite separates contain between 0.6 and 2.0 $\mu\text{g/g}$ Br, with some carbonatitic biotites being below the detection limit of 0.3 $\mu\text{g/g}$ Br (Table 3; Fig. 4a). Higher Br contents in biotite separates were found for a gabbroic sample MSH17 with 4.0 $\mu\text{g/g}$, as well as in the two syenitic samples GM1332 and GM1858 with 3.0 $\mu\text{g/g}$ and 7.7 $\mu\text{g/g}$ Br, respectively. There is no clear correlation between (mean) Cl and Br contents. In biotites from the five syenitic samples, mean/median Cl and Br contents decrease with increasing degree of differentiation to

different extents (Table 3), resulting in an increase of Cl/Br ratio along the sample traverse, although apatites show the opposite trend (Fig. 4b).

3.3. Amphibole

The X_F values in amphiboles, show a very similar pattern as biotites in the same sample (Table 3; Fig. 2c). They are lowest in amphiboles from gabbros and several dioritic and mangeritic rocks and much higher in the monzonite and in syenitic rocks (up to 0.6). As seen for the biotites, amphiboles from syenitic rocks, replacing olivine have higher X_{Mg} and X_F values than amphiboles replacing Fe-Ti oxides (Fig. 5b). Also, X_F correlates negatively with Ti and Al^{IV} (not shown).

In most gabbroic, dioritic and syenitic rocks, amphiboles are relatively low in X_{Cl} (<0.02), with gabbroic samples usually having the lowest Cl contents (Table 3; Fig. 3c). Much higher Cl contents are found in amphiboles from mangeritic rocks and the monzonite ARD16 (0.02–0.08). In most samples, there is no clear correlation between the Cl content of amphibole and its textural type, except for mangeritic sample GM378,

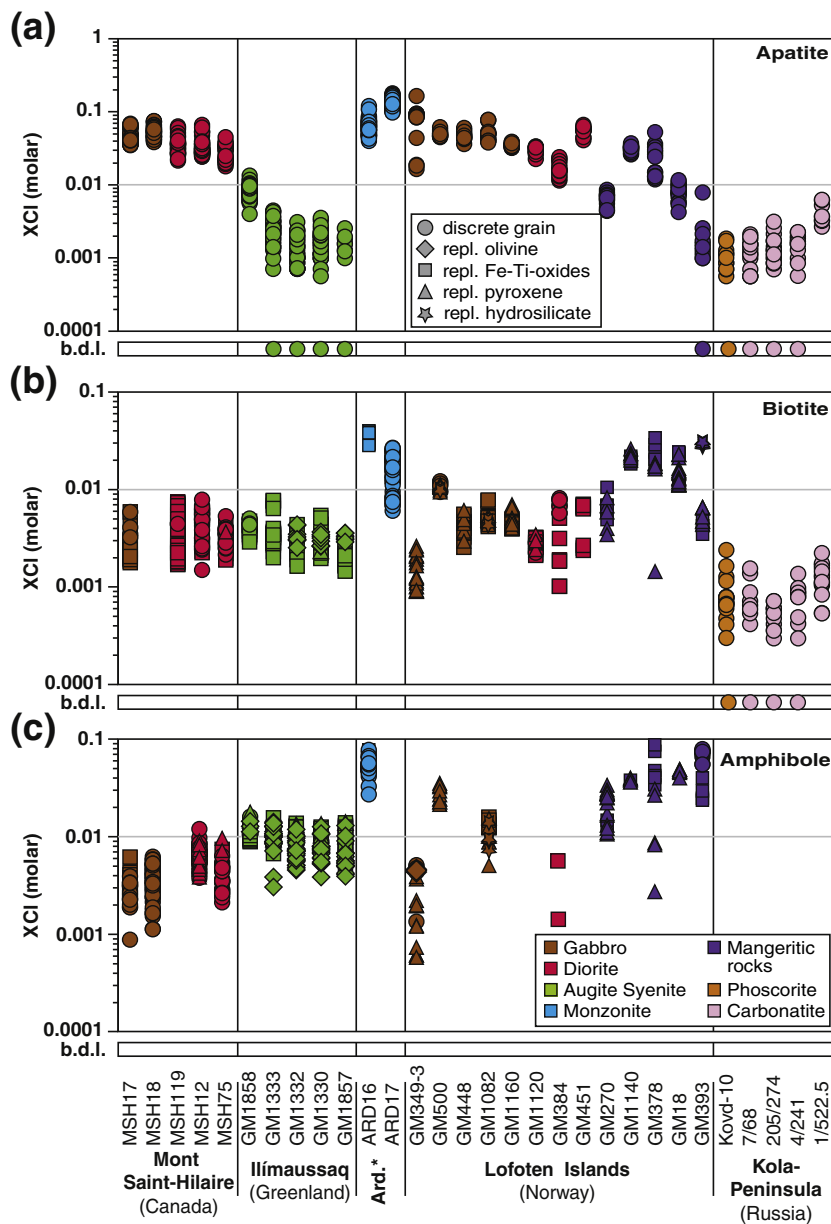


Fig. 3. Molar fraction of Cl (X_{Cl}) in (a) apatite, (b) biotite and (c) amphibole. Samples are grouped by locality and by increasing degree of differentiation. Ard.* = Ardnamurchan (Scotland).

where amphiboles replacing pyroxene show lower X_{Cl} values than those replacing Fe-Ti oxides (Fig. 3c). In mangeritic sample GM393 X_{Cl} values are lower in late-stage amphiboles replacing Fe-Ti oxides than in amphibole grains interpreted as magmatic (Fig. 3c).

Bromine contents in amphibole separates from syenitic rocks could not be quantified due to Fe and Ti pile-ups overlapping with the Br fluorescence line in the TXRF spectra. Amphiboles from Mont Saint-Hilaire samples contain between 0.4 and 1.0 $\mu\text{g/g}$ Br (Table 3; Fig. 4a). As with the apatites and biotites, there is no clear correlation between mean/median Cl and Br contents.

4. Discussion

Apatite is an early magmatic phase in all investigated rock samples, as shown by its sub- to euhedral texture enclosed in, or intergrown with most other early magmatic phases (e.g., pyroxene and Fe-Ti-oxides). In contrast, biotite and amphibole show variable textures in certain samples: Some samples contain relatively large, subhedral to euhedral biotite and/or amphibole. These grains are probably of magmatic origin

and crystallized from evolved melts with a water activity high enough to stabilize biotite and/or amphibole, and probably crystallize slightly later than apatite (e.g., samples from Ardnamurchan and Kola Peninsula, as well as the Lofoten Islands and the biotite-bearing samples from Mont Saint-Hilaire; see above). However, many samples contain mostly fine-grained and anhedral biotite and/or amphibole, that is replacing precursor anhydrous minerals (olivine, pyroxene and Fe-Ti oxides). Their textures indicate that they formed late and crystallized either during late-magmatic or under post-magmatic hydrothermal conditions and therefore clearly after apatite crystallization (e.g., samples from Ilímaussaq, Mont Saint-Hilaire and the Lofoten Islands).

In the following we discuss the partitioning of F and Cl between apatite and biotite using the temperature-dependent model of Zhu and Sverjensky (1992). This will allow us to consider the retention or potential alteration of equilibrium partitioning of F and Cl using the detailed knowledge and consideration of the textural relationships between these two minerals in each sample. Using such models may then reveal if apatite and the texturally different biotites in a given sample are in overall chemical equilibrium with respect to halogens or

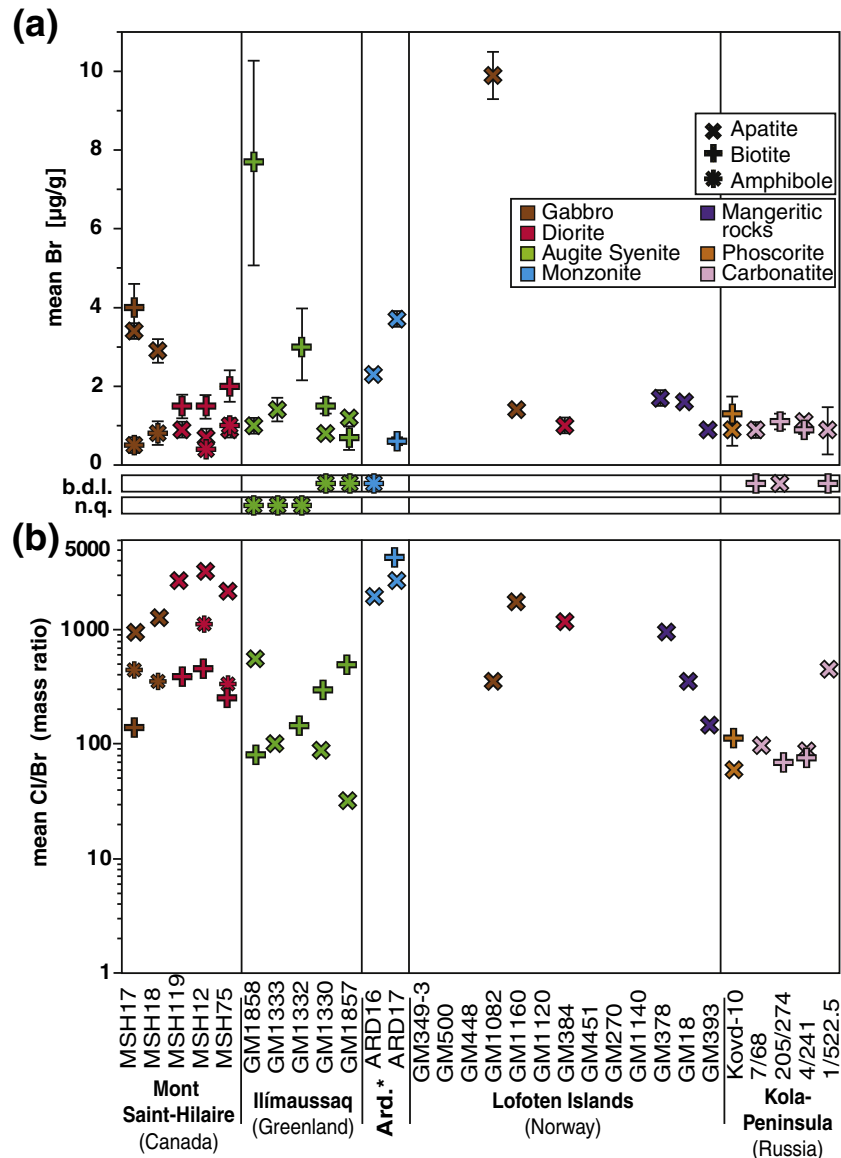


Fig. 4. (a) Bromine contents ($\mu\text{g/g}$) and (b) resulting mean Cl/Br mass ratios from available apatite, biotite and amphibole separates from the different samples. Samples are grouped by locality and by increasing degree of differentiation.

not. Furthermore, this analysis will also allow us to identify potential differences between apatite and biotite concerning their sensitivity to late-stage re-distribution and re-equilibration processes.

In general, the distribution of F and Cl between apatite, biotite and amphibole is governed by several related factors. For example, the halogen abundances in hydroxyl-bearing silicates depend on crystallization temperature (e.g., Leinenhauer and London, 1997) and their major element composition (e.g., Munoz, 1984; Volfinger et al., 1985; Dilles, 1987; Zhu and Sverjensky, 1992), which are in turn influenced by melt composition (including degree of partial melting and differentiation). During hydrothermal events biotite and/or amphibole may replace precursor anhydrous minerals such as olivine, pyroxene, Fe-Ti oxides. The new hydroxyl-bearing silicates may then reflect the fluid composition to varying degrees (e.g., Zhu and Sverjensky, 1992). Eventually, sub-solidus cooling may lead to a re-distribution of halogens (e.g., Brenan, 1993) and interaction with external fluids may cause additional input or removal of halogens at those prevailing conditions (e.g., fluid composition and temperature). As F tends to have less of an affinity for a fluid phase compared to Cl (e.g., Carroll and Webster, 1994; Villemant and Boudon, 1999; Mathez and Webster, 2005;

Webster et al., 2009; Patiño Douce et al., 2011; Zhang et al., 2012; Mangler et al., 2014), it is probably more robust against late-stage fluid-mineral interactions, whereas Cl is relatively more sensitive to these processes.

4.1. Fluorine and chlorine distribution between apatite and magmatic biotite

Biotite of presumably magmatic origin is relatively common in the monzonitic rocks from Ardnamurchan (Scotland) and the carbonatitic rocks from the Kola Peninsula (Russia). In the following we will discuss these two localities in more detail.

For monzonite ARD16, the distribution of F between apatite and biotite yields apparent equilibrium temperatures between 700 to 730 °C, with one pair (apatite in contact with late-stage biotite replacing Fe-Ti oxides) giving a value as low as 620 °C. We consider the latter to reflect late-stage re-equilibration (Fig. 6a). Chlorine data from the same analyses yield similar temperatures (around 750 to 800 °C; Fig. 6b). For comparison, calculations using the mean F and Cl values of apatite and biotite result in similar values (about 700 °C and 800 °C, respectively), suggesting that for the bulk rock the F and Cl distribution

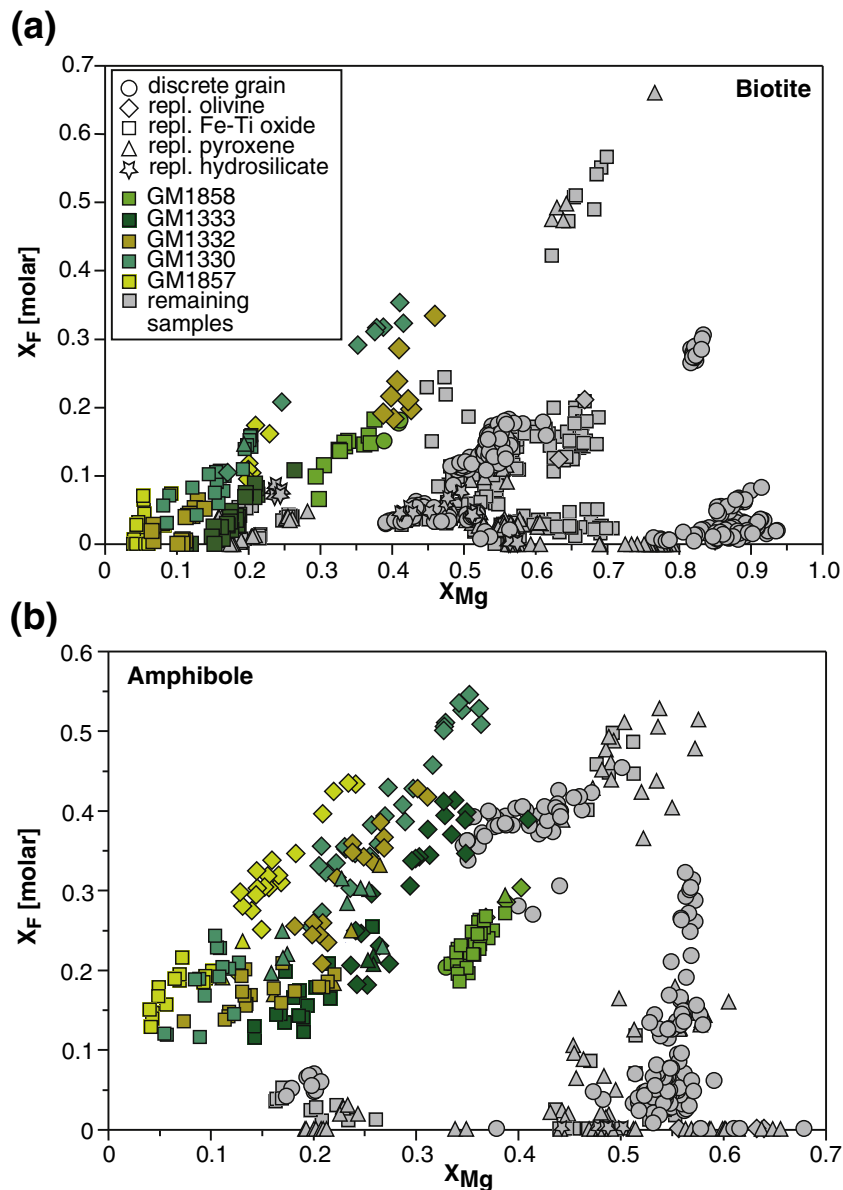


Fig. 5. Molar fraction of F (X_F) in (a) biotite and (b) amphibole as a function of their respective X_{Mg} (given as $Mg/(Mg + Fe + Mn + Ti + Al^{VI})$). For the sake of clarity, only samples from Ilímaussaq are color-coded, all remaining samples are shown in gray. (For interpretation of the references to color in this figure legend, the reader is referred to the web version of this article.)

between apatite and magmatic biotite is largely retained. The distribution of F among apatite–biotite pairs for quartz–monzonite ARD17 gives an apparent equilibrium temperature between 770 and 920 °C (mean of 800 °C), again suggesting equilibration at magmatic conditions (Fig. 6a). However, using the Cl data, much lower mean temperatures of <600 °C are suggested (Fig. 6b). We interpret this as partial redistribution of Cl, probably due to the late-stage or post magmatic removal of Cl from the biotite, which is in cases altered to chlorite at its grain boundaries. This clearly contrasts with F which seems to have retained the original magmatic distribution.

Carbonatite samples from the Kola Peninsula yield apparent equilibration temperatures between apatite and biotite (phlogopite) ranging from ~750 to 600 °C for F, whereas those obtained for Cl are well above 1000 °C (Fig. 6a and b). Note that these data are based on mean F and Cl measurements of apatite and biotite, as contacting apatite–biotite pairs were not available. The large discrepancy between the F and Cl calculations suggests that the two halogens show very different behavior with respect to post-crystallization modifications. Based on the melt inclusion thermometry of Kharlamov et al. (1981) or the calcite–dolomite

geothermometry of Zaitsev and Polezhaeva (1994), the crystallization temperatures for the Kovdor carbonatites are between 940 and 640 °C. Therefore, we assume that temperatures based on the F distribution between apatite and biotite reflect variable diffusive re-equilibration during cooling, as has been suggested by Andersen et al. (1991). The very high temperature estimations based on Cl in these samples are probably in error but may be the consequence of a hydrothermal overprint. We suggest that biotite from these samples was preferably enriched in Cl by equilibration with a late-stage Cl-bearing fluid phase, potentially derived from the carbonatitic melts themselves (e.g., Seifert et al., 2000). Apatite from these samples is relatively low in Cl as observed for most other carbonatites (e.g., Seifert et al., 2000; Patiño Douce et al., 2011; Wang et al., 2014b).

4.2. Fluorine and Cl distribution between apatite and late-stage biotite

Late-stage, biotite, presumably of hydrothermal origin is seen to replace precursor olivine, pyroxene and Fe-Ti oxides in most of the investigated samples. They are, however, especially abundant in the

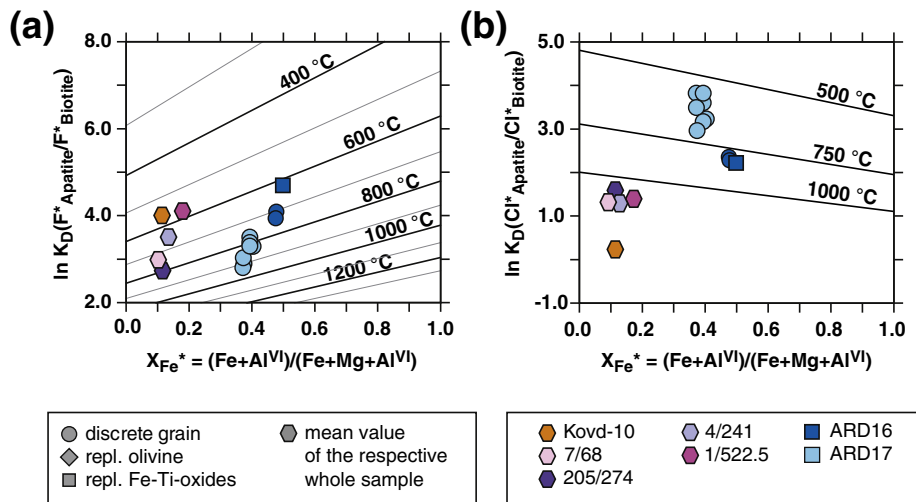


Fig. 6. Equilibration temperatures estimated using F and Cl distribution between contacting apatite–biotite pairs from Ardnamurchan samples (ARD) and estimations based on mean F and Cl values apatites and biotites from individual Kola samples. F^* Apatite = $X_F^{\text{Apatite}} / X_{\text{OH}}^{\text{Apatite}}$, F^* Biotite = $X_F^{\text{Biotite}} / X_{\text{OH}}^{\text{Biotite}}$, Cl^* Apatite = $X_{\text{Cl}}^{\text{Apatite}} / X_{\text{OH}}^{\text{Apatite}}$, Cl^* Biotite = $X_{\text{Cl}}^{\text{Biotite}} / X_{\text{OH}}^{\text{Biotite}}$, $X_{\text{Fe}}^{\text{*Biotite}} = (Fe + Al^{VI}) / (Fe + Mg + Al^{VI})$.

samples from the Ilímaussaq complex. The F and Cl contents of apatite from these Ilímaussaq samples do not show any differences between the textures, which is in contrast to biotite (Fig. 2, 3 and 5). If one assumes, that magmatic apatite re-equilibrated with the late-stage fluid from which the biotite grew, then equilibrium temperatures can be calculated using the halogen distribution. In this case, the calculated equilibrium temperatures between apatite and biotite replacing olivine and Fe-Ti oxide, are largely a function of the variable F and Cl contents and variable $X_{\text{Fe}}^{\text{*Biotite}}$.

For the Ilímaussaq samples, mean F contents of apatite combined with biotite replacing olivine yield systematically higher apparent equilibration temperatures (up to about 1000 °C) compared to biotites replacing Fe-Ti oxides from the same sample (600–700 °C) although there is no textural evidence that biotites replacing olivine originated prior to those replacing Fe-Ti oxides (Fig. 7a). We speculate that this might be related to additional crystal chemical effects influencing the halogen abundances in biotite, which are not accounted for by the Zhu and Sverjensky (1992) model. The temperatures calculated based on F data for biotites replacing Fe-Ti oxides are very similar to temperatures estimated by Markl et al. (2001) for biotite formation in these samples (between 600 and 700 °C). Consequently, we assume that late-magmatic F equilibration of apatite and biotite was largely achieved in this case. The calculated temperatures using mean Cl contents are more variable and also much higher than those obtained by F, resulting in unrealistically high temperatures well above 1000 °C (Fig. 7b). However it should be noted that in some instances the two texturally different apatite–biotite pairs in a given sample do yield relatively similar equilibration temperatures.

Contacting pairs of apatite and late-stage biotite replacing Fe-Ti oxides reveal further heterogeneities on a more local scale: A wide range of temperatures (490–880 °C for F and about 550 up to >1000 °C for Cl) is calculated and the resulting temperatures based on F and Cl data from the same apatite-biotite pair can differ greatly (Fig. 7c and d). Even apatite–biotite pairs in the same samples yield a large apparent temperature range which implies that magmatic apatite and late-stage biotites are probably not well equilibrated for F and Cl. Again, the respective temperatures based on Cl distributions are more variable, and can range to much higher temperatures than those obtained by F distributions. Thus, apatite and biotite are not in overall equilibrium with respect to Cl, which we interpret to result from the relatively mobile character of Cl compared to F in late stage fluids. The same holds true for rocks from the Lofoten Islands, where apparent equilibration temperatures scatter mostly around 700 °C for F and vary widely (from around 550 to >1000 °C) for Cl (Fig. 7 e and f),

with again large differences between F and Cl temperatures in a given sample.

Overall, our data suggest that the post-magmatic re-equilibration of F and Cl between apatite and biotite in the same sample may progress to different extents, even on a mm length scale. Re-equilibration appears to vary for F or Cl in a specific sample. We suggest that Cl may be more easily re-distributed between biotite and a fluid phase compared to F. This appears to be especially true for apatite–biotite pairs where Cl temperatures are (unrealistically) high compared to those obtained from the F concentrations. In this case, we suggest that biotite might have gained Cl during a hydrothermal overprint, whereas apatite did not. Consequently, late-stage biotites have not equilibrated their Cl with the magmatic apatite, due to insufficient time for equilibration (e.g., cooling and diffusion). In rare cases, where calculated equilibrium temperatures based on F and Cl are similar and typically reflect temperatures lower than around 800 °C, we assume that late-stage re-equilibration with respect to F and Cl between apatite and biotite was achieved. It is, however, obvious that equilibrium temperature estimations based on Cl data have to be regarded with great caution and F data are much more reliable.

4.3. Fluorine and chlorine distribution between apatite and amphibole

The partitioning of F among apatite-amphibole pairs shows no clear relationship with $X_{\text{Fe}}^{\text{*Amphibole}}$ and suggests a clear preference for apatite over amphibole (Fig. 8a). For Cl, however, a roughly negative correlation with $X_{\text{Fe}}^{\text{*Amphibole}}$ is apparent (Fig. 8b), where more Fe-rich amphiboles (replacing olivine) favor the incorporation of Cl over apatite. As no correlation is observed within individual samples, we assume that this might reflect the higher mobility of Cl that is overwhelming any crystal chemical effect. It is also possible that any equilibrium distribution cannot be resolved, due to overall low Cl contents in both minerals.

4.4. Fluorine and chlorine distribution among co-genetic biotite-amphibole pairs

The preferential uptake of F for amphibole over biotite is apparent in the replacement textures involving Fe-Ti oxides from syenites at Ilímaussaq, mostly for samples where $X_{\text{Fe}}^{\text{*Biotite}}$ is larger than $X_{\text{Fe}}^{\text{*Amphibole}}$ (Fig. 8c). In some gabbroic, monzonitic and mangeritic rocks where amphibole and biotite are presumably of early or late magmatic origin, there is generally no obvious preference of F for either amphibole or

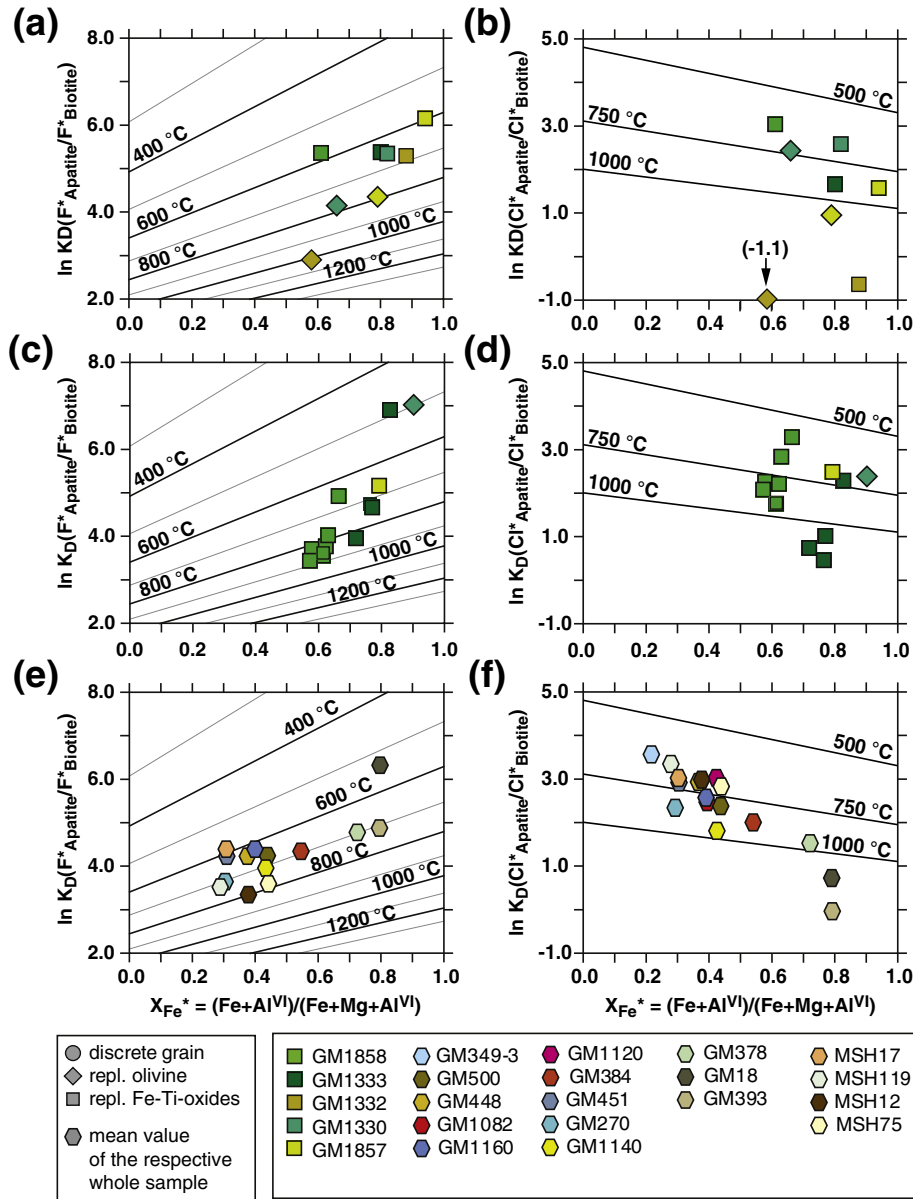


Fig. 7. (a) and (b): Equilibration temperatures based on mean apatite and biotite values for F and Cl from individual Ilimaussaq samples. (c) and (d): Equilibration temperatures estimated using contacting apatite–biotite pairs based on F and Cl data. (e) and (f): Equilibration temperatures estimated based on mean F and Cl values in apatites and biotites, for individual Lofoten Island samples.

biotite. We suggest that this indicates limited F fractionation between biotite and amphibole at relatively high temperatures (magmatic origin). Significant fractionation may only occur at cooler, late-stage, and probably sub-solidus conditions. This appears plausible as the two mineral groups have relatively similar structures concerning the local environment (e.g., arrangement of OH-position with respect to octahedral cations; Volfinger et al., 1985). In contrast, the heavier, larger radius and more incompatible Cl, shows a general preference for amphibole over biotite, as indicated by almost all our data, largely independent of textural occurrence (Fig. 8d). It is possible that the apparent preference of Cl for amphibole could be a post-magmatic effect caused by the relative mobility of Cl compared to F, and slight differences concerning the re-equilibration behavior between the two hydroxyl-bearing silicates. In this case only biotite-amphibole pairs with more or less equal distribution of Cl would represent the retained magmatic equilibrium. Interestingly, some previous studies on the distribution of F and Cl between biotite and amphibole have yielded similar, and partly contradicting distribution patterns in gabbroic, dioritic, monzonitic, granodioritic, granitic and syenitic rocks

(e.g., Gillberg, 1964; Ekström, 1972; Westrich, 1981; Zhang et al., 2012; Teiber et al., 2014). However, the lack of any detailed textural relationships for the respective biotite-amphibole pairs in these studies makes it difficult to compare these previous results with ours.

4.5. Bromine contents and Cl/Br ratios in apatite, biotite and amphibole

Our data imply that Br contents for apatite are either similar (Kola samples), lower (Mont Saint-Hilaire and Ilímaussaq samples) or higher (Ardnamurchan samples) than those of coexisting biotite but are generally of a similar magnitude, consistent with the previous data of Teiber et al. (2014). Overall, the Cl/Br mass ratios for apatites, biotites, and amphiboles show considerable variation between around 30 and 4000 (Fig. 4b), with apatites generally having higher ratios than hydroxyl-bearing silicates from the same sample, and amphibole being higher than biotite. Among the Mont Saint-Hilaire samples, Cl/Br ratios are generally highest for apatite, intermediate for amphibole and lowest for biotite in any given sample. Ignoring the different textural interpretations,

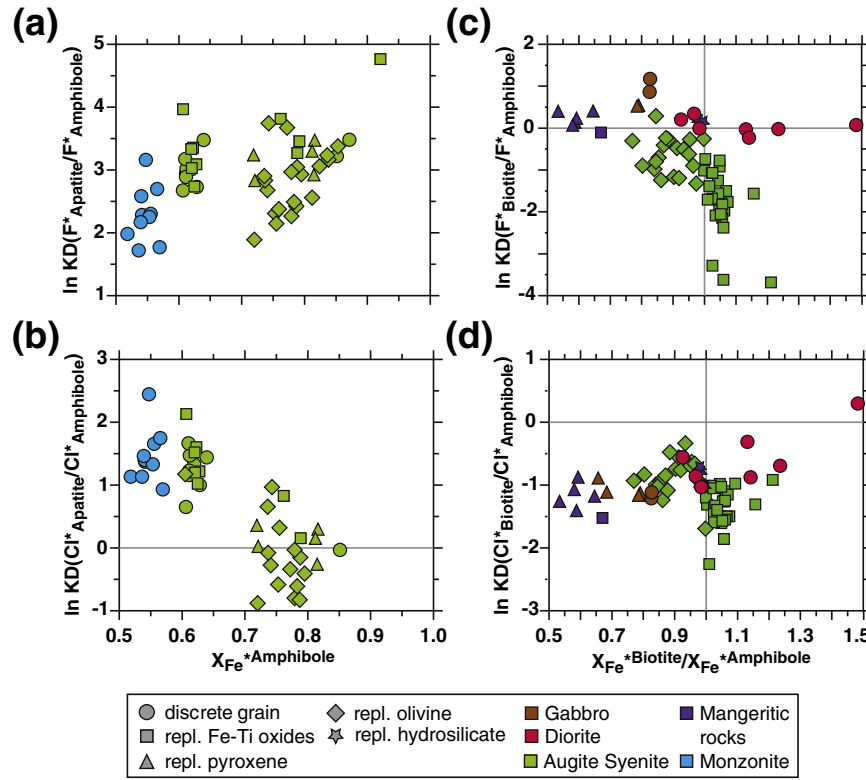


Fig. 8. Distribution of (a) F and (b) Cl between contacting apatite–amphibole pairs, and between contacting biotite–amphibole pairs for F (c) and Cl (d). $F^*_{\text{Amphibole}} = X_{\text{F}}^{\text{Amphibole}} / X_{\text{OH}}^{\text{Amphibole}}$, $Cl^*_{\text{Amphibole}} = X_{\text{Cl}}^{\text{Amphibole}} / X_{\text{OH}}^{\text{Amphibole}}$, $X_{\text{Fe}}^*_{\text{Amphibole}} = (\text{Fe} + \text{Al}^{VI}) / (\text{Fe} + \text{Mg} + \text{Al}^{VI})$; F^*_{Apatite} , Cl^*_{Apatite} , F^*_{Biotite} and Cl^*_{Biotite} see caption of Fig. 6.

this may indicate that these three minerals can fractionate Cl from Br to different extents.

In the syenitic rocks from the Ilímaussaq complex, Cl/Br mass ratios of apatites decrease from about 600 in the relatively fine-grained and probably faster cooled marginal sample (GM1858) to values as low as 30 in the coarse-grained innermost sample (GM1857), which probably cooled much slower (Fig. 4b). In the same samples, however, Cl/Br ratios of texturally late and presumably hydrothermal biotites show the opposite trend, increasing from about 80 to 500 (Fig. 4b). Based on our observations (see above) and previous studies, which showed that magmatic differentiation is unlikely to produce large variations in Cl/Br ratios (e.g., Wang et al., 2014a and references therein), we consider it unlikely that the decreasing trend in Cl/Br ratios for apatite represents undisturbed magmatic values. Because of its relatively fast cooling rate, apatite from the marginal sample (GM1858) has the highest potential to preserve their initial Cl/Br ratio. The Cl/Br ratio in apatite for this sample is much higher than that of biotite, which is consistent with the systematics observed for the Mont Saint-Hilaire samples and the Cl concentration in these apatites is higher than in the other samples (see above). Consequently, this would also imply that all apatites lost some of their initial Br during cooling, diffusive re-equilibration or later hydrothermal overprint. Assuming that biotites from all samples crystallized from homogeneous fluid with a constant Cl/Br ratio at approximately the same temperature, roughly similar Cl/Br for these biotites would be expected, which contradicts the observed increase of Cl/Br ratios (Fig. 4b). Therefore, we propose that, biotites crystallized from a fluid phase, which evolved over time towards the inner part of the magmatic body. As Cl is probably more compatible in biotite than Br (due of its smaller ionic radius; see above), biotite should always have a higher Cl/Br ratio than the coexisting fluid phase. Consequently, biotite fractionation should progressively decrease the Cl/Br ratio of the residual fluid phase. Later biotite crystallizing in the inner parts of the complex should therefore show lower Cl/Br ratios, which contradicts our data (Fig. 4b).

One possible explanation is that a later influx of external fluid might be responsible for the observed Cl/Br systematics in biotite. Groundwater or saline lake water or seawater have been proposed as the external fluid source (Marks et al., 2007), which might have carried significant amounts of Cl and Br causing variable low-temperature redistribution of Cl and Br between biotite, apatite and fluid, depending on a number of factors such as fluid-rock ratio, temperature, etc. Although Cl and Br show very similar behavior during magmatic high-temperature processes, the Cl/Br ratio of minerals may be strongly altered by low-temperature re-distribution processes such as diffusion and/or hydrothermal overprint.

5. Conclusions

Our detailed observations on the distribution of F and Cl between apatite, biotite and amphibole for a range of texturally determined crystallization sequences in a range of plutonic rocks show that apatite may retain magmatic halogen abundances. F seems to be less affected than Cl by any subsequent re-distribution processes during cooling (e.g., diffusion or hydrothermal overprint). The larger Cl anion seems to be more easily mobilized and re-distributed during hydrothermal processes, especially in biotite and amphibole. Therefore, the distribution of F and Cl between apatite and biotite may also be a very sensitive indicator of post-magmatic processes such as fluid overprint. Only detailed textural evaluation combined with extensive spatially resolved analyses can be used to constrain either primary (magmatic) or late-stage (hydrothermal) halogen abundances in the melts or fluids from which the minerals crystallized.

In accordance with previous studies, our data show that apatite always incorporates more F and Cl than coexisting biotite and amphibole. However, previous studies and our work on the distribution of F and Cl between biotite and amphibole also demonstrate some partly contradictory distribution patterns. Potential fractionation effects of F

and Cl between these two structurally similar silicate mineral groups are relatively small compared to halogen fractionation between apatite and either biotite or amphibole. Further investigation, and in particular experimental studies are needed to better constrain and quantify the distribution of halogens between biotite and coexisting amphibole.

The Cl/Br mass ratios in a given rock sample are usually highest for apatite, intermediate for amphibole and lowest for biotite. This indicates that these three minerals may fractionate Cl from Br to variable extents. As Br is probably the most incompatible of the three halogens investigated in this study, such re-equilibration effects are expected to result in a general loss of Br from the affected minerals, depending on factors like cooling rate and/or intensity of hydrothermal overprint.

Acknowledgments

We are very grateful to Simone Kaulfuß for careful sample preparation. The detailed comments and suggestions of Chao Zhang, Anatoly Zaitsev, Richard Brooker and Editor Nelson Eby to help improve this manuscript are highly acknowledged. Funding of this work by the Deutsche Forschungsgemeinschaft (grant MA 2563/3-1), the RFBR (grant 15-05-02116), and the St. Petersburg State University (Grant 3.38.224.2015) are gratefully acknowledged.

Appendix A. Supplementary data

Supplementary data to this article can be found online at <http://dx.doi.org/10.1016/j.lithos.2015.02.015>.

References

- Aiuppa, A., Baker, D.R., Webster, J.D., 2009. Halogens in volcanic systems. *Chemical Geology* 263, 1–18.
- Andersen, T., Austrheim, H., Dilles, J.H., 1991. Temperature-HF fugacity trends during crystallization of calcite carbonatite magma in the Fen complex, Norway. *Mineralogical Magazine* 55, 81–94.
- Armstrong, J.T., 1991. Quantitative elemental analysis of individual microparticles with electron beam instruments. In: Heinrich, K.F.J., Newbury, D.E. (Eds.), *Electron Probe Quantitation*. Plenum Press, New York & London, pp. 261–315.
- Arzamastsev, A.A., Bea, F., Glaznev, V.N., Arzamasteva, L.V., Montero, P., 2001. Kola alkaline province in the Paleozoic: evolution of primary mantle magma composition and magma generation conditions. *Russian Journal of Earth Science* 3, 1–32.
- Boyce, J.W., Hervig, R.L., 2008. Magmatic degassing histories from apatite volatile stratigraphy. *Geology* 36, 63–66.
- Breiter, K., Siebel, W., 1995. Granitoids in the Rozvadov Pluton, Western Bohemia and Oberpfalz. *Geologische Rundschau* 84, 506–519.
- Brenan, J.M., 1993. Partitioning of fluorine and chlorine between apatite and aqueous fluids at high pressure and temperature: implications for the F and Cl content of high P-T fluids. *Earth and Planetary Science Letters* 117, 251–263.
- Brenan, J., 1994. Kinetics of fluorine, chlorine and hydroxyl exchange in fluorapatite. *Chemical Geology* 110, 195–210.
- Bureau, H., Keppler, H., Métrich, N., 2000. Volcanic degassing of bromine and iodine: experimental fluid/melt partitioning data and applications to stratospheric chemistry. *Earth and Planetary Science Letters* 183, 51–60.
- Carroll, M.R., Webster, J.D., 1994. Solubilities of sulfur, noble gases, nitrogen, chlorine, and fluorine in magmas. In: Carroll, M.R., Holloway, J.R. (Eds.), *Reviews in Mineralogy 30 – Volatiles in Magmas*. Mineralogical Society of America, Washington, D.C., pp. 231–280.
- Chevychelov, V.Y., Botcharnikov, R.E., Holtz, F., 2008. Experimental study of fluorine and chlorine contents in mica (biotite) and their partitioning between mica, phonolite melt, and fluid. *Geochemistry International* 46, 1081–1089.
- Corfu, F., 2004. U-Pb age, setting and tectonic significance of the anorthosite–mangerite–charnockite–granite suite, Lofoten–Vesterålen, Norway. *Journal of Petrology* 45, 1799–1819.
- Currie, K.K., Eby, G.N., Gittins, J., 1986. The petrology of the Mont Saint Hilaire complex, southern Quebec: an alkaline gabbro–peralkaline syenite association. *Lithos* 19, 65–81.
- Darbyshire, F.A., Eaton, D.W., Frederiksen, A.W., Ertolahti, L., 2007. New insights into the lithosphere beneath the Superior Province from Rayleigh wave dispersion and receiver function analysis. *Geophysical Journal International* 169, 1043–1068.
- Dilles, J.H., 1987. Petrology of the Yerington Batholith, Nevada; evidence for evolution of porphyry copper ore fluids. *Economic Geology* 82, 1750–1789.
- Eby, G.N., 1985. Sr and Pb isotopes, U and chemistry of the alkaline Montereian and White Mountain igneous provinces, eastern North America. *Geochimica et Cosmochimica Acta* 49, 1143–1153.
- Ekström, T.K., 1972. The distribution of fluorine among some coexisting minerals. *Contributions to Mineralogy and Petrology* 34, 192–200.
- Emeleus, C.H., Bell, B.R., 2005. The Paleogene Volcanic Districts of Scotland. Fourth ed. British Geological Survey, Nottingham, p. 214.
- Foland, K.A., Jiang-Feng, C., Gilbert, L.A., Hofmann, A.W., 1988. Nd and Sr isotopic signatures of Mesozoic plutons in northeastern North America. *Geology* 16, 684–687.
- Förster, H.J., Tischendorf, G., Trumbull, R.B., Gottesmann, B., 1999. Late-collisional granites in the Variscan Erzgebirge, Germany. *Journal of Petrology* 40, 1613–1645.
- Frindt, S., Trumbull, R.B., Romer, R.L., 2004. Petrogenesis of the Gross Spitzkoppe topaz granite, central western Namibia: a geochemical and Nd–Sr–Pb isotope study. *Chemical Geology* 206, 43–71.
- Frost, B.R., Chamberlain, K.R., Schumacher, J.C., 2000. Spheine (titanite): phase relations and role as a geochronometer. *Chemical Geology* 172, 131–148.
- Fuge, R., 1977. On the behaviour of fluorine and chlorine during magmatic differentiation. *Contribution to Mineralogy and Petrology* 61, 245–249.
- Geldmacher, J., Haase, K.M., Devey, C.W., Garbe-Schönberg, C.D., 1998. The petrogenesis of tertiary cone-sheets in Ardnamurchan, NW Scotland: petrological and geochemical constraints on crustal contamination and partial melting. *Contributions to Mineralogy and Petrology* 131, 196–209.
- Gieré, R., Sørensen, S.S., 2004. Allanite and other REE-rich epidote-group minerals. *Reviews in Mineralogy and Geochemistry* 56, 431–493.
- Gillberg, M., 1964. Halogens and hydroxyl contents of micas and amphiboles in Swedish granitic rocks. *Geochimica et Cosmochimica Acta* 28, 495–516.
- Gioncada, A., Orlando, P., Vezzoli, L., Omarini, R.H., Mazzuoli, R., Lopez-Azarevich, V., Sureda, R., Azarevich, M., Acocella, V., Ruch, J., 2014. Topaz magmatic crystallization in rhyolites of the Central Andes (Chivinar volcanic complex, NW Argentina): constraints from texture, mineralogy and rock chemistry. *Lithos* 184–187, 62–73.
- Goldoff, B., Webster, J.D., Harlov, D.E., 2012. Characterization of fluor-chlorapatites by electron probe microanalysis with a focus on time-dependent intensity variation of halogens. *American Mineralogist* 97, 1103–1115.
- Icenhower, J.P., London, D., 1997. Partitioning of fluorine and chlorine between biotite and granitic melt: experimental calibration at 200 MPa H₂O. *Contributions to Mineralogy and Petrology* 127, 17–29.
- Ionov, D.A., Griffin, W.L., O'Reilly, S.Y., 1997. Volatile-bearing minerals and lithophile trace elements in the upper mantle. *Chemical Geology* 141, 153–184.
- Kharlamov, Y.S., Kudryavtseva, G.P., Garanin, V.K., Korennova, N.G., Moskalyuk, A.A., Sandomirskaia, S.M., Shugurova, N.A., 1981. Origin of the carbonatites of the Kovdor deposit. *International Geology Review* 23, 865–880.
- Krasnova, N.I., Balaganskaya, E.G., Garcia, D., 2004. Kovdor – classic phoscorites and carbonatites. In: Wall, F., Zaitsev, A.N. (Eds.), *Phoscorites and Carbonatites from Mantle to Mine: the Key Example of the Kola Alkaline Province*. Mineralogical Society Series, 10. Mineralogical Society, London, pp. 99–132.
- Krumrei, T.V., Pernicka, E., Kaliwoda, M., Markl, G., 2007. Volatiles in a peralkaline system: abiogenic hydrocarbons and F–Cl–Br systematics in the naujaite of the Ilímaussaq intrusion, South Greenland. *Lithos* 95, 298–314.
- Larsen, L.M., Sørensen, H., 1987. The Ilímaussaq intrusion–progressive crystallization and formation of layering in an agpaitic magma. *Geological Society, London, Special Publications* 30, 473–488.
- Léger, A., Rebett, C., Webster, J., 1996. Cl-rich biotite and amphibole from Black Rock Forest, Cornwall, New York. *American Mineralogist* 81, 495–504.
- Mangler, M.F., Marks, M.A.W., Zaitsev, A.N., Eby, G.N., Markl, G., 2014. Halogens (F, Cl and Br) at Oldoinyo Lengai volcano (Tanzania): Effects of magmatic differentiation, silicate–natrocarnobatite melt separation and surface alteration of natrocarnobatite. *Chemical Geology* 365, 43–53.
- Markl, G., 2001. REE constraints on fractionation processes of massive-type anorthosites on the Lofoten Islands, Norway. *Mineralogy and Petrology* 72, 325–351.
- Markl, G., Frost, B.R., 1999. The origin of anorthosites and related rocks from the Lofoten Islands, Northern Norway: II. Calculation of parental liquid compositions for anorthosites. *Journal of Petrology* 40, 61–77.
- Markl, G., Höhndorf, A., 2003. Isotopic constraints on the origin of AMCG-suite rocks on the Lofoten Islands, N Norway. *Mineralogy and Petrology* 78, 149–171.
- Markl, G., Piazolo, S., 1998. Halogen-bearing minerals in syenites and high-grade marbles of DronningMaud Land, Antarctica: monitors of fluid compositional changes during latemagmatic fluid–rock interaction processes. *Contributions to Mineralogy and Petrology* 132, 246–268.
- Markl, G., Frost, B.R., Bucher, K., 1998. The origin of anorthosites and related rocks from the Lofoten Islands, Northern Norway: I. Field relations and estimation of intrinsic variables. *Journal of Petrology* 39, 1425–1452.
- Markl, G., Marks, M., Schwinn, G., Sommer, H., 2001. Phase equilibrium constraints on intensive crystallization parameters of the Ilímaussaq complex, South Greenland. *Journal of Petrology* 42, 2231–2258 (Markl, G., 2001).
- Marks, M., Markl, G., 2001. Fractionation and assimilation processes in the alkaline augite syenite unit of the Ilímaussaq Intrusion, South Greenland, as deduced from phase equilibria. *Journal of Petrology* 42, 1947–1969.
- Marks, M., Markl, G., 2015. The Ilímaussaq complex, South Greenland. (xxx–xxx). In: Charlier, B., Namur, O., Latypov, R., Tegner, C. (Eds.), *Layered Intrusions*. Springer, Dordrecht (in press).
- Marks, M.A.W., Vennemann, T., Siebel, W., Markl, G., 2004a. Nd-, O-, and H-isotopic evidence for complex, closed-system fluid evolution of the peralkaline Ilímaussaq intrusion, South Greenland. *Geochimica et Cosmochimica Acta* 68, 3379–3395.
- Marks, M., Halama, R., Wenzel, T., Markl, G., 2004b. Trace element variations in clinopyroxene and amphibole from alkaline to peralkaline syenites and granites: implications for mineral–melt trace-element partitioning. *Chemical Geology* 211, 185–215.
- Marks, M.A.W., Rudnick, R.L., McCammon, C., Vennemann, T., Markl, G., 2007. Arrested kinetic Li isotope fractionation at the margin of the Ilímaussaq complex, South Greenland: evidence for open-system processes during final cooling of peralkaline igneous rocks. *Chemical Geology* 246, 207–230.

- Marks, M.A.W., Wenzel, T., Whitehouse, M.J., Loose, M., Zack, T., Barth, M., Worgard, L., Krasz, V., Eby, G.N., Stosnach, H., Markl, G., 2012. The volatile inventory (F, Cl, Br, S, C) of magmatic apatite: an integrated analytical approach. *Chemical Geology* 291, 241–255.
- Marty, B., Tolstikhin, I., Kamensky, I.L., Nivin, V., Balaganskaya, E., Zimmermann, J.L., 1998. Plume-derived rare gases in 380 Ma carbonatites from the Kola region (Russia) and the argon isotopic composition in the deep mantle. *Earth and Planetary Science Letters* 164, 179–192.
- Mason, R.A., 1992. Models of order and iron-fluorine avoidance in biotite. *Canadian Mineralogist* 20, 343–354.
- Mathez, E.A., Webster, J.D., 2005. Partitioning behavior of chlorine and fluorine in the system apatite–silicate melt–fluid. *Geochimica et Cosmochimica Acta* 69, 1275–1286.
- Munoz, J.L., 1984. F–OH and Cl–OH exchange in micas with applications to hydrothermal ore deposits. *Reviews in Mineralogy and Geochemistry* 13, 469–493.
- O'Driscoll, B., 2007. The centre 3 layered gabbro intrusion, Ardnamurchan, NW Scotland. *Geological Magazine* 144, 897–908.
- O'Reilly, S.Y., Griffin, W.L., 2000. Apatite in the mantle: implications for metasomatic processes and high heat production in Phanerozoic mantle. *Lithos* 53, 217–232.
- Patino Douce, A.E., Roden, M., Chaumba, J., Chris Fleisher, C., Yodzinski, G., 2011. Compositional variability of terrestrial mantle apatites, thermodynamic modeling of apatite volatile contents, and the halogen and water budgets of planetary mantles. *Chemical Geology* 288, 14–31.
- Piccoli, P., Candela, P., 2002. Apatite in igneous systems. In: Kohn, M.L., Rakovan, J., Hughes, J.M. (Eds.), *Reviews in Mineralogy and Geochemistry – Phosphates: Geochemical, Geobiological, and Materials Importance* 48. Mineralogical Society of America, Washington, D.C., pp. 255–292.
- Pyle, D.M., Mather, T.A., 2009. Halogens in igneous processes and their fluxes to the atmosphere and oceans from volcanic activity: a review. *Chemical Geology* 263, 110–121.
- Schilling, J., Frost, B.R., Marks, M.A.W., Wenzel, T., Markl, G., 2011a. Fe–Ti oxide – silicate (QUILF-type) equilibria in feldspathoid-bearing systems. *American Mineralogist* 96, 100–110.
- Schilling, J., Marks, M.A., Wenzel, T., Vennemann, T., Horváth, L., Tarassoff, P., Jacob, D.E., Markl, G., 2011b. The magmatic to hydrothermal evolution of the intrusive Mont Saint-Hilaire complex: insights into the late-stage evolution of peralkaline rocks. *Journal of Petrology* 52, 2147–2185.
- Seifert, W., Kämpf, H., Wasternack, J., 2000. Compositional variation in apatite, phlogopite and other accessory minerals of the ultramafic Delitzsch complex, Germany: implication for cooling history of carbonatites. *Lithos* 53, 81–100.
- Shannon, R.D., 1976. Revised effective ionic radii and systematic studies of interatomic distances in halides and chalcogenides. *Acta Crystallographica* 32, 751–767.
- Speer, J.A., 1984. Micas in igneous rocks. In: Bailey, S.W. (Ed.), *Reviews in Mineralogy – Micas* 13. Mineralogical Society of America, Washington, D.C., pp. 299–356.
- Stock, M.J., Humphreys, M.S.C., Smith, V.C., Johnson, R.D., Pyle, D.M., EIMF, 2015. New constraints on electron-beam induced halogen migration in apatite. *American Mineralogist* 100, 281–293.
- Stormer, J.C., Carmichael, I.S.E., 1971. Fluorine-hydroxyl exchange in apatite and biotite: a potential igneous geothermometer. *Contribution to Mineralogy and Petrology* 31, 121–131.
- Stormer, J.C., Pierson, M.L., Tacker, R.C., 1993. Variation of F and Cl X-ray intensity due to anisotropic diffusion in apatite during electron microprobe analysis. *American Mineralogist* 78, 641–648.
- Teertstra, D.K., Sherriff, B.L., 1997. Substitutional mechanisms, compositional trends and the end-member formulae of scapolite. *Chemical Geology* 136, 233–260.
- Teiber, H., Marks, M.A.W., Wenzel, T., Siebel, W., Altherr, R., Markl, G., 2014. The distribution of halogens (F, Cl, Br) in granitoid rocks. *Chemical Geology* 374–375, 92–109.
- Upton, B.G.J., 2013. Tectono-magmatic evolution of the younger Gardar southern rift, South Greenland. *Geological Survey of Denmark and Greenland Bulletin* 29, 124.
- Villemant, B., Boudon, G., 1999. H₂O and halogen (F, Cl, Br) behaviour during shallow magma degassing processes. *Earth and Planetary Science Letters* 168, 271–286.
- Volfinger, M., Robert, J.L., Vielzeuf, D., Neiva, A.M.R., 1985. Structural control of the chlorine content of OH-bearing silicates (micas and amphiboles). *Geochimica et Cosmochimica Acta* 49, 37–48.
- Wall, F., Zaitsev, A.N., 2004. Phoscorites and carbonatites from mantle to mine: the key example of the Kola Alkaline Province. *The Mineralogical Society of Great Britain & Ireland*, London, p. 498.
- Walsh, J.N., 1975. Clinopyroxenes and biotites from the Centre III igneous complex, Ardnamurchan, Argyllshire. *Mineralogical Magazine* 40, 332–345.
- Walsh, J.N., Henderson, P., 1977. Rare earth element patterns of rocks from the centre 3 igneous complex, Ardnamurchan, Argyllshire. *Contributions to Mineralogy and Petrology* 60, 31–38.
- Wang, L., Marks, M.A.W., Keller, J., Markl, G., 2014a. Halogen variations in alkaline rocks from the Upper Rhine Graben (SW Germany): insights into F, Cl and Br behavior during magmatic processes. *Chemical Geology* 380, 133–144.
- Wang, L., Marks, M.A.W., Wenzel, T., von der Handt, A., Keller, J., Teiber, H., Markl, G., 2014b. Apatites from the Kaiserstuhl Volcanic Complex, Germany: new constraints on the relationship between carbonatite and associated silicate rocks. *European Journal of Mineralogy* 26, 397–414.
- Webster, J.D., Holloway, J.R., 1990. Partitioning of F and Cl between magmatic hydrothermal fluids and highly evolved granitic magmas. *Geological Society of America Special Papers* 246, 21–34.
- Webster, J.D., Tappin, C.M., Mandeville, C.W., 2009. Partitioning behavior of chlorine and fluorine in the system apatite–melt–fluid. II: felsic silicate systems at 200 MPa. *Geochimica et Cosmochimica Acta* 73, 559–581.
- Westrich, H.R., 1981. F–OH exchange equilibria between mica–amphibole mineral pairs. *Contributions to Mineralogy and Petrology* 78, 318–323.
- Willmore, C.C., Boudreau, A.E., Kruger, F.J., 2000. The halogen geochemistry of the Bushveld Complex, Republic of South Africa: implications for chalcophile element distribution in the lower critical zones. *Journal of Petrology* 41, 1517–1539.
- Zaitsev, A., Polezhaeva, L., 1994. Dolomite–calcite textures in early carbonatites of the Kovdor ore deposit, Kola peninsula, Russia: their genesis and application for calcite–dolomite geothermometry. *Contributions to Mineralogy and Petrology* 115, 339–344.
- Zaitsev, A.N., Williams, C.T., Jeffries, T.E., Strekopytov, S., Moutte, J., Ivashchenko, O.V., Spratt, J., Petrov, S.V., Wall, F., Seltmann, R., Borozdin, A.P., 2014. Rare earth elements in phoscorites and carbonatites of the Devonian Kola Alkaline Province, Russia: examples from Kovdor, Khibina, Vuoriyari and Tury Mys complexes. *Ore Geology Reviews* 61, 204–225.
- Zhang, C., Holtz, F., Ma, C., Wolff, P.E., Li, X., 2012. Tracing the evolution and distribution of F and Cl in plutonic systems from volatile-bearing minerals: a case study from the Liujiawa pluton (Dabie orogen, China). *Contributions to Mineralogy and Petrology* 164, 859–879.
- Zhu, C., Sverjensky, D.A., 1991. Partitioning of F–Cl–OH between minerals and hydrothermal fluids. *Geochimica et Cosmochimica Acta* 55, 1837–1858.
- Zhu, C., Sverjensky, D.A., 1992. F–Cl–OH partitioning between biotite and apatite. *Geochimica et Cosmochimica Acta* 55, 3435–3467.
- Zirner, A.L., Marks, M.A.W., Wenzel, T., Jacob, D.E., Markl, G., submitted to *Chemical Geology*. Rare Earth Elements in apatite as a monitor of crystallization and metasomatic processes: the Ilímaussaq intrusion, South Greenland, as a type example.